Geosci. Model Dev. Discuss., 4, 137–196, 2011
www.geosci-model-dev-discuss.net/4/137/2011/
doi:10.5194/gmdd-4-137-2011

Geoscientific Model Development Discussions

Modeling and computation of effective emissions: a position paper

R. Paoli[1], **D. Cariolle**[1,2], **and R. Sausen**[3]

[1]Sciences de l'Univers au CERFACS, CERFACS/CNRS, URA 1875, Toulouse, France
[2]Météo France, Toulouse, France
[3]Deutsches Zentrum für Luft- und Raumfahrt (DLR), Institut für Physik der Atmosphäre, Oberpfaffenhofen, Germany

Received: 7 December 2010 – Accepted: 17 December 2010 – Published: 19 January 2011

Correspondence to: R. Paoli (roberto.paoli@cerfacs.fr)

Published by Copernicus Publications on behalf of the European Geosciences Union.

Abstract

An important issue in the evaluation of the environmental impact of emissions from concentrated sources such as transport modes, is to understand how processes occurring at the scales of exhaust plumes can influence the physical and chemical state of the atmosphere at regional and global scales. Indeed, three-dimensional global circulation models or chemistry transport models generally assume that emissions are instantaneously diluted into large-scale grid boxes, which may lead, for example, to overpredict the efficiency of NO_x to produce ozone. In recent times, various methods have been developed to incorporate parameterizations of plume processes into global models that are based either on the correction of the original emissions or on the introduction of subgrid reaction rates in the models. This paper provides a review of the techniques proposed so far in the literature to account for local conversion of emissions in the plume, as well as the implementation of these techniques into atmospheric codes.

1 Introduction

In order to study the impact of anthropogenic emissions of trace gases on the global-scale atmospheric composition, global chemistry transport models (CTMs) or global climate-chemistry models (CCMs) are usually applied, e.g., Cess et al. (1990), Roeckner et al. (1996), Kraaøbl et al. (1999), Zeng and Pyle (2003), Hauglustaine et al. (2004). Depending on model resolution the grid boxes have sizes of few degrees in latitudinal and longitudinal directions, and of several hundred metres to few kilometres in vertical direction. The emissions are usually provided by emission inventories on a 2-D latitude-longitude grid, e.g., on a regular $1^\circ \times 1^\circ$ grid, in the case of surface emissions (Lawrence and Crutzen, 1999; Eyring et al., 2007) and on a 3-D latitude-longitude-altitude grid in the case of emissions in the free atmosphere such as emissions from aviation or from lightning (Velders et al., 1994; Brasseur et al., 1998; Meijer et al., 2000). When doing this, one implicitly makes the assumption that the emissions are

GMDD
4, 137–196, 2011

not subject to chemical or physical processes apart from dilution and that they are instantaneously homogeneously distributed into model grid boxes; at least these effects are assumed negligible.

However, in many cases large line-shaped source, e.g., aircraft, ships or motorways, and large point sources, such as big factories of power plants, the emissions result in local concentrations significantly (up to several orders of magnitude) larger than the background concentrations (Schlager et al., 1997, 2006). Most of the chemical transformations processes and some of the physical processes non-linearly depend on the concentrations of the species involved (Danilin et al., 1994; Brasseur et al., 1996; Lin et al., 1998; Jaeglé et al., 1998; von Glasow et al., 2003; Song et al., 2003). Therefore, we can expect an impact of the processes occurring while the species are diluted into areas of the size of global model grid boxes. For instance, aircraft NO_x emissions may result in a higher production of ozone when they get instantaneously mixed with background, since this does not account for the effect that the efficiency of NO_x to produce O_3 decreases with increasing NO_x concentration (Meijer et al., 1997; Kasibhatla et al., 2003).

In recent times different approaches have been made to tackle the problem, in particular in the context of studying the impact of aviation on the global-scale atmospheric composition, e.g., Meijer et al. (1997), Petry et al. (1998), Kraabøl et al. (2002), Cariolle et al. (2009), but also when considering ship emissions (Franke et al., 2008; Huszar et al., 2010). All of them are parameterizations, i.e., they do not explicitly model the processes occurring during the initial dilution and dispersion of the emissions, they rather mimic the effect of the emissions on the large-scale variables such as mean box concentrations of chemical species. The various approaches differ in the theoretical concepts how to mimic the large-scale effects of local emissions. Basically, three different concepts have been published so far: Effective Emissions Indexes (EEI), Emission Conversion Factors (ECF) and Effective Reaction Rates (ERR). In these approaches either the emissions themselves are modified or the relevant reactions rates in the chemical formulae.

GMDD
4, 137–196, 2011

This study is organized as follows: the general conservation equations for global models in the presence of emissions from concentrated sources are briefly presented in Sect. 2. Section 3 gives an overview of the various models currently used to represent the plume chemical processes. Section 4 presents the main principles of plume parameterizations for use in global models, while Sect. 5 reviews the results of their implementation into either GCM/CTM or regional models. Finally, a synthetic comparison among the different methods is presented and conclusions are drawn in Sect. 6.

2 General formulation of large-scale models in the presence of exhaust plumes

In order to analyze the different techniques developed to integrate the parameterization of reactive plumes into global models, it can be useful to examine the global mass balance equations starting from the basic mass conservation laws for a mixture of reacting species in a fluid:

$$\frac{\partial C_k}{\partial t} + \nabla\cdot(C_k\boldsymbol{u}) + \nabla\cdot(D_k\nabla C_k) = E_k + \omega_k\,, \quad k = 1,\ldots,N_\mathrm{s} \tag{1}$$

where N_s is the number of species, $\boldsymbol{u}$ is the fluid velocity, while C_k, D_k, E_k and ω_k are, respectively, the concentration, the molecular diffusion coefficient, the emission rate and chemical sources of species k. The chemical sources account for all reaction, $j=1,\ldots,N_\mathrm{r}$, contributing to the production/removal of species k:

$$\omega_k = \sum_{j=1}^{N_\mathrm{r}} \Delta\nu_{k_j} K_j C_{k_{j_1}}^{\nu_{k_{j_1}}} C_{k_{j_2}}^{\nu_{k_{j_2}}} \equiv \omega_k\left(C_1,\ldots,C_{N_\mathrm{s}}\right) \tag{2}$$

where K_j is the rate of reaction j, $\Delta\nu_{k_j}$ is the difference between the forward and backward stoichiometric coefficients of species k in reaction j, and k_{j_1} and k_{j_2} denote the two species involved in reaction j, with $\nu_{k_{j_1}}$ and $\nu_{k_{j_2}}$ the corresponding (forward) stoichiometric coefficients.

GMDD
4, 137–196, 2011

Large-scale atmospheric models do not directly solve Eq. (1) but an "average" form of these equations, where average can be interpreted either in a statistical sense as an ensemble mean (Reynolds average), or as a grid average over a large computational cell (Galmarini et al., 2008). In the latter case, one can define a grid-average for any variable φ as:

$$\overline{\varphi}(\boldsymbol{x},t) = \frac{1}{V}\int_V \varphi(\boldsymbol{y},t)\,d\boldsymbol{y} \tag{3}$$

where V and $\boldsymbol{x}$ are the volume and the center of the cell, respectively, and a perturbation around the mean as

$$\varphi'(\boldsymbol{x},t) = \varphi(\boldsymbol{x},t) - \overline{\varphi}(\boldsymbol{x},t)\,. \tag{4}$$

Using Eq. (4), Eq. (1) become

$$\frac{\partial \overline{C}_k}{\partial t} + \nabla\cdot\left(\overline{C}_k\overline{\boldsymbol{u}}\right) + \nabla\cdot\left(D_t\nabla\overline{C}_k\right) = \overline{E}_k + \overline{\omega}_k \tag{5}$$

where the classical Boussinesq approximation has been made for the unclosed turbulent or sub-grid scale diffusion: $\overline{C}'_k\overline{\boldsymbol{u}}' = -D_{\text{turb}}\nabla\overline{C}_k$ and $D_t \equiv D_k + D_{\text{turb}}$ (in practice $D_t \simeq D_{\text{turb}}$ in the atmosphere). Introducing the total derivative operator:

$$\frac{D\varphi}{Dt} \equiv \frac{\partial\varphi}{\partial t} + \nabla\cdot\left(\overline{\boldsymbol{u}}\varphi\right) + \nabla\cdot(D_t\varphi) \tag{6}$$

for any variable φ, Eq. (5) can be recast as

$$\frac{D\overline{C}_k}{Dt} = \overline{E}_k + \overline{\omega}_k\,. \tag{7}$$

The grid-averaged emission rate $\overline{E}_k$ in the right-hand side of Eq. (7) can be reconstructed using inventories of aircraft or ship emissions along prescribed air or see corridors:

$$\overline{E}_k = \mathrm{EI}_k\overline{S}_{\mathrm{f}} \tag{8}$$

GMDD
4, 137–196, 2011

with EI_k the species emission index and S_f the fuel consumption per unit volume. The grid-averaged chemical source $\overline{\omega}_k$ contains various non-linear sub-grid scale terms involving C_k and K_j. The sub-grid contribution due to the reaction rates can be neglected because of their weak dependence on temperature, i.e., $\overline{K_j \varphi} \simeq \overline{\varphi}\,\overline{K}_j$ for any variable φ. Hence, averaging Eq. (2) and using Eqs. (3) and (4) yields

$$\overline{\omega}_k = \sum_{j=1}^{N'_r} \Delta\nu_{k_j} \overline{K}_j \overline{C}_{k_{j_1}} + \sum_{j=1}^{N''_r} \Delta\nu_{k_j} \overline{K}_j \overline{C}_{k_{j_1}} \overline{C}_{k_{j_2}} + \sum_{j=1}^{N''_r} \Delta\nu_{k_j} \overline{K}_j \overline{C'_{k_{j_1}} C'_{k_{j_2}}} \tag{9}$$

where N'_r and N''_r (with $N_r \equiv N'_r + N''_r$) indicate the number of uni-molecular reactions ($\nu_{k_{j_1}}$=1, $\nu_{k_{j_2}}$=0) and bi-molecular reactions ($\nu_{k_{j_1}} = \nu_{k_{j_2}} = 1$), respectively. (Chemical reactions with higher molecularity are not common in the atmosphere and will not be considered here). The first two summations in the right-hand side of Eq. (9) contain grid-averaged variables that are directly transported by the global model. On the other hand, the last summation contains non-linear sub-grid scale fluctuations of species concentrations $\overline{C'_{k_{j_1}} C'_{k_{j_2}}}$ which are in general unknown. If chemical species are not well mixed within a computational cell (as in the case of emissions from concentrated sources) these terms cannot be neglected and have to be modeled or parameterized. Two main strategies can then be developed. The first strategy consists in modifying the emissions to take into account the sub-grid plume transformations that cannot be resolved by the global model. Denoting by

$$\overline{\omega}_k\left(\overline{C}_1, \ldots, \overline{C}_{N_s}\right) \equiv \sum_{j=1}^{N'_r} \Delta\nu_{k_j} \overline{K}_j \overline{C}_{k_{j_1}} + \sum_{j=1}^{N''_r} \Delta\nu_{k_j} \overline{K}_j \overline{C}_{k_{j_1}} \overline{C}_{k_{j_2}} \tag{10}$$

the contributions of chemical sources that depend exclusively on transported grid-averaged quantities and using Eq. (9), Eq. (7) can be formally recast as

$$\frac{D\overline{C}_k}{Dt} = \overline{E}_k^{\text{eff}} + \overline{\omega}_k\left(\overline{C}_1, \ldots, \overline{C}_{N_s}\right) \tag{11}$$

GMDD
4, 137–196, 2011

where $\overline{E}_k^{\text{eff}}$ are modified or "effective" emissions. The second strategy consists in parameterizing the sub-grid chemical sources such that Eq. (7) becomes

$$\frac{D\overline{C}_k}{Dt} = \overline{E}_k + \overline{\omega}_k\left(\overline{C}_1, \ldots, \overline{C}_{N_s}\right) + \sum_{j=1}^{N_r''} \Delta\nu_{k_j} \overline{K}_j^{\text{eff}} \overline{C}_{k_{j_1}} \overline{C}_{k_{j_2}} \tag{12}$$

where $\overline{K}_j^{\text{eff}}$ are "effective" reaction rates. Whatever strategy is chosen, Eqs. (11) or (12) now contain averaged ("bar") quantities that are known at run time by the global model, all the external modeling effort is condensed into either $\overline{E}_k^{\text{eff}}$ or $\overline{K}_j^{\text{eff}}$.

It is worth observing that these parameterizations are not meant to reproduce the actual evolution of exhaust plumes. In fact, the resolution used in large-scale models (a few hundred kilometers) does not allow to resolve the dynamical and physico-chemical processes occurring at the scales of the plume (which range from meters to a few kilometers once trace gases get mixed with background). This is shown for example in Fig. 1 which sketches the dispersion of exhausts in aircraft plumes according to the representation proposed by Gerz et al. (1998). The process is initially driven by the dynamics of the wake vortices generated by the airplane (primary vortex pair). During the first few seconds after emission, the exhaust material is trapped around the wake vortices (jet regime), which later start to sink by the mutually induced downward velocity (vortex regime). Part of the exhausts is detrained into a secondary vortex pair that forms due to the buoyancy force induced by atmospheric stratification while the majority of exhausts undergoes a complex instability process that leads to the vortex break-up, turbulence production and release of exhausts in the atmosphere (dissipation regime). In the final diffusion regime the exhausts get diluted to background level via atmospheric processes (turbulence, radiation transport, etc.) usually within 2 to 12 h.

Ship plumes are another example of plumes from concentrated sources (see the sketch in Fig. 2). In this case the exhausts are released at the ship stack and initially

GMDD
4, 137–196, 2011

disperse in the vertical direction before reaching the top of the marine boundary layer. Afterwards, the dispersion takes place mostly in the horizontal direction until complete dilution. This process can strongly depend on the background conditions and in particular on the typology of the boundary layer as well as the initial buoyancy flux at the stack of the ship (Chosson et al., 2008).

The most accurate way to model the evolution of reactive species in such complex scenarios is to rely on three-dimensional large-eddy simulations (LES) that cover the entire lifetime of the plume. However, although feasible, these simulations are still extremely demanding of computational resources – CPU power, memory and data storage – especially if several cases have to be run for a number of different conditions. High-resolution LES of reactive wakes may require up to several million grid-points for tens of seconds to minutes plume age simulations (Lewellen and Lewellen, 2001a,b; Paoli et al., 2004; Chosson et al., 2008; Paugam et al., 2010). As detailed in the following sections, the alternative to such expensive three-dimensional simulations is to rely on plume parameterizations that provide surrogates for $\overline{E}_k^{\text{eff}}$ or $\overline{K}_j^{\text{eff}}$. Then, data from detailed LES or from experiments can be used to calibrate these parameters.

3 Representation of plume processes

This section examines the different models that have been developed in the literature to parameterize the processes occurring in plumes like those sketched in Figs. 1 and 2. The common feature of these models is that they use a finite (generally small) number of parameters to represent the structure of the plume and the distribution of exhausts within it. These parameters evolve in time and obey ordinary differential equations (i.e., they do not explicitly depend on space), so in this sense all these models are zero-dimensional. Examples of key parameters are the mean concentration within the plume in Gaussian plume models, or the mean concentration within radial sectors of the plume in Multilayered Plume models that will be described below. An important aspect that differentiate these models is the way of representing the mixing in the

GMDD
4, 137–196, 2011

interior of the plume and the entrainment of ambient air. To avoid confusion with the symbols C_k defined in Sect. 2 that pertain to large-scale Chemical Transport Models, the concentrations obtained from small-scale plume models will be denoted by low-case symbols c_k.

3.1 Instantaneous Dispersion (ID)

This simple parameterization represents the way emissions are usually handled in global models: the emissions are instantaneously diluted to the scales of a large control volume (e.g., the computational cell of a global model). Since this parameterization does not require any plume specification, only one set of ordinary differential equations for the mean concentrations c_k^{ID} within the control volume is then sufficient to represent the process:

$$\frac{dc_k^{\mathrm{ID}}}{dt} = E_{k,t_0} + \omega_k\left(c_1^{\mathrm{ID}},\ldots,c_{N_s}^{\mathrm{ID}}\right) \tag{13}$$

where the first term in the right-hand side means that emissions are non-zero only at time $t=t_0$ while the chemical sources ω_k obey the same law as in Eq. (2).

3.2 Single plumes

In the Single Gaussian Plume model, two sets of ordinary differential equations are solved: one for the mean concentration inside the plume c_k^{p} and one for the background concentration c_k^{a}:

$$\frac{dc_k^{\mathrm{p}}}{dt} = E_{k,t_0} + \omega_k\left(c_1^{\mathrm{p}},\ldots,c_{N_s}^{\mathrm{p}}\right) + \left(c_k^{\mathrm{p}} - c_k^{\mathrm{a}}\right)\frac{1}{V_{\mathrm{p}}}\frac{dV_{\mathrm{p}}}{dt} \tag{14}$$

$$\frac{dc_k^{\mathrm{a}}}{dt} = \omega_k\left(c_1^{\mathrm{a}},\ldots,c_n^{\mathrm{a}}\right) \tag{15}$$

GMDD
4, 137–196, 2011

where V_p denotes the volume of the plume. In the case of aircraft emissions, plume is asymmetric and anisotropic at cruise altitude because of atmospheric stratification and wind shear. A classical way of defining the dispersion of the plume is using a matrix of variances that follow a Gaussian distribution in the plane perpendicular to the flight path: σ_h and σ_v for the horizontal and vertical variances, and σ_s the diagonal term of the matrix accounting for the deformation of the plume by vertical wind shear. Analytical solutions for these variances were obtained by Konopka (1995):

$$\sigma_h^2 = \sigma_{h,0}^2 + 2\left(s\sigma_{s,0}^2 + D_h\right)t + \left(2sD_s + s^2 + \sigma_{v,0}^2\right)t^2 + \frac{2}{3}s^2 D_v t^3 \quad (16)$$

$$\sigma_v^2 = \sigma_{v,0}^2 + 2D_v t \quad (17)$$

$$\sigma_s^2 = \sigma_{s,0}^2 + \left(s\sigma_{v,0}^2 + 2D_s\right)t + sD_v t^2 \quad (18)$$

where D_v, D_h and D_s denote the vertical, horizontal, and shear diffusion coefficients, respectively, while s denotes the wind shear. The subscript 0 in the above equations refer to a plume age t_0 when the expansion of the plume can be approximated by a pure diffusion process (typically the beginning of the diffusion regime as discussed in the previous section). The emissions in Eq. (14) should also be interpreted as already diluted at the spatial scale of the plume corresponding to t_0. Table 1 summarizes the values of coefficients in Eqs. (16)–(18) obtained from in situ measurements (Schumann et al., 1995). The volume of the plume and the cross-sectional area A_p can be obtained from Eqs. (16)–(17) as (Konopka, 1995):

$$A_p(t) = n^2\pi\left(\sigma_h^2\sigma_v^2 - \sigma_s^4\right)^{1/2} \quad (19)$$

$$V_p(t) = A_p(t)L_{path} \quad (20)$$

where L_{path} denotes a reference length along flight direction, e.g., the distance flown by the aircraft per second, L_{path}=250 m at cruise speed (Kraabøl et al., 2000b), while n determines the fraction of the Gaussian distribution containing the exhaust and sets

GMDD
4, 137–196, 2011

the width of the plume. For example, choosing n=2 corresponds to incorporate 98% of exhaust (Petry et al., 1998).

In the case of ship emissions, the vertical and horizontal variances of the plume (with respect to the ship direction) can be derived by matching Gaussian solutions to empirical dispersion parameters (Seinfeld and Pandis, 2006). For example, Hanna et al. (1985) and Song et al. (2003) determined σ_h and σ_v by the standard deviations of turbulent velocity fluctuations and the integral time scales of turbulence whereas von Glasow et al. (2003) proposed the simpler expressions

$$\sigma_h = \sigma_{h,0} \left(\frac{t}{t_0} \right)^{\alpha} \tag{21}$$

$$\sigma_v = \sigma_{v,0} \left(\frac{t}{t_0} \right)^{\beta} \tag{22}$$

where subscript 0 identifies a reference time, for example t_0=1 s after emission, while α and β are are the plume expansion rates that depend on the specific atmospheric conditions. von Glasow et al. (2003) also provided "best guest values" of 0.75 and 0.6 for α and β, respectively, based on the work by Durkee et al. (2000) (see also Table 2). Once the variances are specified, the ship plume area can be reconstructed using Eq. (19) (with $\sigma_s \equiv 0$), in particular taking $n=1/\sqrt{8}$, gives $A_p = \pi/8 \sigma_h \sigma_v$ which corresponds to a semi-elliptical cross-section (von Glasow et al., 2003).

The Multilayered Plume model was first developed by Melo et al. (1978) and Vilà-Guerau de Arellano et al. (1990) as a generalization of the single plume model for aircraft emissions. The plume is indeed divided into N_l concentric rings or layers in order to represent the concentration distributions (see Fig. 3). A number of rings $4<N_l<16$ has been typically used in the literature (Melo et al., 1978; Meijer, 2001; Kraabøl et al., 2000b; Vohralik et al., 2008). In this model, Eqs. (14)–(15) are replaced by the following set of equations for the mean concentration c_k^l inside each ring l of the

GMDD
4, 137–196, 2011

plume:

$$\frac{dc_k^l}{dt} = E_{k,t_0} + \omega_k\left(c_1^l,\ldots,c_{N_s}^l\right) + f\left(c_k^1,\ldots,c_k^{N_l};A_1,\ldots,A_{N_l}\right)\frac{1}{V_p}\frac{dV_p}{dt} \quad (23)$$

where A_l and $V_l \equiv A_l L_{path}$ are, respectively, the area and the volume of the ring; $V_p = \sum_{l=1}^{N_l} V_l$, while f is a function that parameterizes the mixing of species across different layers of the plume (Meijer, 2001; Kraabøl et al., 2000b). The concentration in the outermost layer corresponds to the ambient concentration, $c_k^{N_l} \equiv c_k^a$, while the overall mean concentration in the plume is given by

$$c_k^p = \frac{\sum_{l=1}^{N_l} c_k^l V_l}{\sum_{l=1}^{N_l} V_l} \equiv \frac{\sum_{l=1}^{N_l} c_k^l V_l}{V_p}. \quad (24)$$

It is interesting to rewrite the last term in the right-hand side of Eqs. (14) or (23) in terms of the entrainment rate ω_E or its inverse, the entrainment time τ_E:

$$\omega_E \equiv \frac{1}{\tau_E} = \frac{1}{V_p}\frac{dV_p}{dt} \quad (25)$$

which represents the instantaneous expansion rate of the plume whose evolution can be computed analytically using Eqs. (16)–(20). The above equation suggests that in the limit $\tau_E \to 0$, the plume concentration c_k^p relaxes instantaneously towards the ambient concentration c_k^a (see Eq. 15 or 23): in this case the single plume models degenerate into the instantaneous dispersion model and Eq. (13) is recovered. It is worth remarking that τ_E is a measure of the *instantaneous* dilution of the plume and, as such, it does not provide any indication about the *lifetime* of the plume, which is a measure of the timescale over which exhausts can be considered diluted to background level. As discussed in the next section, this point is particularly relevant to the parameterization of plume processes into global models whose spatial and temporal resolutions do not allow to reproduce the entire evolution of the plume.

GMDD
4, 137–196, 2011

3.2.1 Choice of the plume lifetime

In the literature, various definitions have been proposed for the plume lifetime t_p. Petry et al. (1998) suggested to take

$$t_p \equiv t_{ref} \tag{26}$$

where t_{ref} is the "dispersion" time, i.e., the time when the plume reaches the dimensions of a reference area A_{ref}, for example the 2-D latitude-longitude grid box of a global model (see Fig. 4). For typical grid resolutions employed in CTM, $A_{ref} \simeq 5 \times 10^7 m^2$ and $t_{ref} \simeq 18$ h although this value strongly depends on the actual resolution of the global model and on the dispersion parameters of the atmosphere. Meijer (2001), Karol et al. (2000) and Kraabøl et al. (2000b) defined the plume lifetime as

$$t_p \equiv t_{mix} \tag{27}$$

where t_{mix} represents the "mixing" time, i.e., the time when the NO_x chemical conversion rate in the plume and in the ambient air are sufficiently close (in practice, when the difference falls below a small threshold value, see Fig. 5). As shown by Karol et al. (2000), this time can vary significantly with the background conditions, the characteristics of the atmospheric turbulence and the location of the plume, e.g., if it is inside or outside a flight corridor. Kraabøl et al. (2002) chose the life time as the minimum between the dispersion and the mixing times:

$$t_p \equiv \mathrm{MIN}(t_{ref}, t_{mix}) \,. \tag{28}$$

A rather different approach has been developed by Cariolle et al. (2009) to represent plume dilution. This is based on the fact that the non-linear chemical processes within the plume are efficient up to a threshold value of exhaust concentration c_{lim}. The plume is then constituted by the air masses with concentration in excess with respect to c_{lim}:

$$V_p = V : c - c_{lim} > 0 \,, \tag{29}$$

GMDD
4, 137–196, 2011

$$m_p^* = \int_{V_p} (c - c_{lim}) dV_p \quad (30)$$

where c indicates the concentration of a conserved species in the plume (e.g., NO_x) and V is a control volume. The excess of exhaust mass m_p^* decreases monotonically in time until it gets to zero at $t = t_{lim}$ as sketched in Fig. 6. This time is then taken as the plume lifetime:

$$t_p = t_{lim} . \quad (31)$$

All the definitions of plume lifetime introduced above, Eqs. (26)–(31), implicitly assume that plumes do not overlap. However, in regions of dense traffic individual plumes can merge and the air masses with high exhaust concentration can have longer lifetime. Meilinger et al. (2005) determined the average plume encounter time t_{enc} hours for the North Atlantic Flight Corridor (NAFC), which is an "objective" definition of plume lifetime in the sense that it does not depend on a specific plume or global model but only on the average aircraft flux density (see Fig. 7). The Single Plume or the Multilayered Plume models should be strictly valid only if the diffusion process is efficient enough for t_{ref} or t_{mix} to be lower than the average plume encounter time t_{enc}. This is generally satisfied: for example, Petry et al. (1998) and Meijer (2001) found $t_{ref} \sim 18$ h and $t_{mix} \sim 15$ h, respectively, whereas $t_{enc} \sim 48$ h (Meilinger et al., 2005). Similarly, in the approach proposed by Cariolle et al. (2009), the plume size and lifetime depend on the mixing properties of the atmosphere and on the threshold value c_{lim} chosen for exhaust concentration. In the case of NO_x, this threshold is $c_{lim} \sim 1$ ppb and the corresponding $t_{lim} \sim 15$ h, which, again, is much lower than t_{enc}.

4 Parameterizations of emissions into global models

The plume models described above and 3-D large-eddy simulations can represent the evolution of the plume at the different levels of sophistication. However, because of the

GMDD
4, 137–196, 2011

difference of scales and representation of physical processes, it would be unrealistic to integrate all the information carried by these small-scale models into large-scale CTM. For these reasons, a number of simpler parameterizations have been developed in the literature that attempt to reconstruct a limited number of parameters from small-scale models that can be efficiently used in CTM.

4.1 Effective Emission Indexes (EEI)

The concept of Effective Emission Indexes (EEI) was introduced by Petry et al. (1998) to provide corrections to instantaneous dispersion (ID) models where the emitted species are distributed instantaneously and homogeneously over the grid-box of large-scale models. Effective emissions are determined by varying the emissions obtained with ID models and by comparing the corresponding results obtained with a Single Plume model (or Multilayered plume model) at the plume lifetime $t_p \equiv t_{ref}$ (see Eq. 26) as sketched in Fig. (8). This procedure provides the variation $\Delta c_k^*(t_0)$ that has to be added to the initial excess of concentration over background,

$$c_k^{*ID}(t_0) \equiv c_k^p(t_0) - c_k^a \,, \tag{32}$$

to retrieve the correct value a $t=t_p$. Once this variation is known, the initial excess of concentration $c_k^{*ID}(t_0)$ is replaced by the corrected excess $c_k^{*ID_{corr}}(t_0)$ defined as:

$$c_k^{*ID_{corr}}(t_0) = c_k^{*ID}(t_0) + \Delta c_k^*(t_0) \,. \tag{33}$$

To guarantee the conservation of the modified nitrogen mass of emitted species like NO_x, an effective emission index of non-emitted or secondary species like ozone has to be introduced. Then, to obtain maximum agreement with plume model results, a minimization procedure is applied to the root mean square deviation F:

$$F = \sqrt{\sum_{i=1}^{n} \left[\frac{c_k^{*ID_{corr}}(t_p) - c_k^*(t_p)}{c_k^*(t_p)} \right]^2} \,. \tag{34}$$

GMDD
4, 137–196, 2011

For emitted species k_e like NO_x, the Effective Emission Index is obtained by simply rescaling the standard Emission Index so as to take into account the correction in Eq. (33):

$$\mathrm{EEI}_{k_e}(t_0) = \left[1 + \delta_{\mathrm{rel}}(k_e)\right] \mathrm{EI}_{k_e} \tag{35}$$

where

$$\delta_{\mathrm{rel}}(k_e) \equiv \frac{\Delta c^*_{k_e}(t_0)}{c^{*\mathrm{ID}}_{k_e}(t_0)} \tag{36}$$

is the relative correction of exhaust species concentrations. For secondary or non-emitted species k_{ne} like ozone, Effective Emission Indices are defined by rescaling the NO_x Emission Index as

$$\mathrm{EEI}_{k_{ne}}(t_0) = \delta_{\mathrm{rel}}(k_{ne})\mathrm{EI}_{\mathrm{NO_x}} \tag{37}$$

where

$$\delta_{\mathrm{rel}}(k_{ne}) = \frac{W_{k_{ne}}}{W_{\mathrm{NO_x}}} \frac{\Delta c^*_{k_{ne}}(t_0)}{c^{*\mathrm{ID}}_{\mathrm{NO_x}}(t_0)} \tag{38}$$

is the relative correction of secondary species concentrations with respect to NO_x, while W_k denotes the molecular weight of species k. Petry et al. (1998) computed the EEI by means of their Single Plume model that employs the Chemistry Module for the Lower Stratosphere and the Troposphere (CHEST). This chemical mechanism is based on the EURAD model system (Hass, 1991) and considers the transformations of 160 species by 160 homogeneous gas phase collision reactions and 26 photolysis reactions (Stockwell, 1986; Stockwell et al., 1990). Figure 9 shows a good agreement between the $c^{*\mathrm{ID_{corr}}}_k(t_p)$ and $c^*_k(t_p)$ for the absolute changes of some key species, meaning that that Eq. (33) allows the concentrations of the instantaneous dispersion model to recover the correct plume model concentrations at the end of the plume

GMDD
4, 137–196, 2011

lifetime. Figure 10 reports the time evolution of Δc_k^* for different background conditions. As a general remark, Petry et al. (1998) found that the corrections to the concentration obtained with the standard ID method can vary significantly, depending on release time and the degree pollution of the background environment. In particular, negative NO_y and ozone effective emission indexes were obtained for some specific release times.

Franke et al. (2008) recently applied the EEI method to ship emissions using the plume dispersion formulation by Song et al. (2003) and the photochemical box model MECCA (Sander et al., 2005), which includes 160 gas-phase reactions in addition to 116 aqueous, 61 heterogeneous and 42 equilibrium reactions for sulfur and sea-salt aerosols. Both primary emissions and secondary emissions for ozone and H_2O_2 and the corrections of NO_x were balanced by effective emissions of HNO_3, PAN and sea-salt aerosol nitrate. They observed that the original NO_x emissions were reduced by about 3%, while ozone and H_2O_2 were, respectively, reduced by 700% and increased by 5% the amount of emitted NO_x (see Fig. 11). As expected, the relative emission indexes are always negative due to the fact that they correct the ozone overestimation of the ID model box. The effective emissions of O_3 are largest for release times during day and smallest during night.

Once the EEI are computed, the "effective" emissions in the CTM mass balance equations are reconstructed as

$$\overline{E}_k^{\text{eff}} = \text{EEI}_k(t_0)\overline{S}_{\text{f}} \tag{39}$$

which formally replaces Eq. (8).

4.2 Emission Conversion Factors (ECF)

The method of Emission Conversion Factor (ECF) proposed by Meijer et al. (1997), Meijer (2001) attempts to determine the local conversions of the emitted species on the same plume, rather than forcing emissions from ID model to follow those of SP models, as sketched in Fig. 12. For emitted species, Meijer (2001) introduced the

GMDD
4, 137–196, 2011

excess of mass over background as the difference between the number of molecules in the control volume with and without the aircraft plume:

$$m^*_{k_e}(t) = V_p(t)\left(c^p_{k_e}(t) - c^a_{k_e}(t)\right) \quad (40)$$

while, for non-emitted species the excess of mass is given by

$$m^*_{k_{ne}}(t) = V_p(t)c^p_{k_{ne}}(t)\,. \quad (41)$$

The ECF is then defined as the ratio between the emissions of species k and that of all nitrogen oxides NO_y (which is constant in time since NO_y are chemically conserved):

$$ECF_k(t) = \frac{m^*_k(t)}{m^*_{NO_y}(t)} = \frac{c^p_k(t) - c^a_k(t)}{c^p_{NO_y}(t) - c^a_{NO_y}(t)}\,. \quad (42)$$

The Multilayered Plume model used to compute the ECF is described in detail in Meijer (2001). The photochemical mechanism for the troposphere contains 44 species and 103 reactions, and is adapted from Strand and Hov (1994), with gas-phase reaction rates taken from De More et al. (1997) and microphysics from Kärcher (1997). The background conditions correspond to typical values encountered along the NAFC at an altitude of about 10.5 km (250 hPa), at different times (respectively 8 a.m. and 12 a.m.) and different seasons (January and July). The ECF are reported in Fig. 13: as expected, ECF_{NO_x} decreases while ECF_{O_3} increases as NO_x is converted in the plume. For all cases, the net chemical rates of NO_x and O_3 in the plume shows large destruction rate during the first hours, whereafter the net rate slowly converges to the net rate in the ambient air (around 10 h). A value of $t_p \equiv t_{mix} = 15$ h (see Eq. 27) was then suggested as a conservative choice for the plume lifetime.

A similar approach was used by Kraabøl et al. (2000b) and Kraabøl and Stordal (2000). One difference is that their chemistry scheme, taken from Kraaøbl et al. (1999), contains 66 species and 170 reactions, providing a complete description of the free-atmosphere. In addition, their analysis showed that the NO_x conversion rates

GMDD
4, 137–196, 2011

were most sensitive to the diurnal, seasonal and latitudinal variations of background conditions (see e.g., Fig. 14), and then suggested that such variations should be taken into account for the integration in global models. Vohralik et al. (2008) recently tested the ECF technique and confirmed the strong dependence of NO_x conversion into NO_y on altitude, latitude and seasonal variations (see Fig. 15).

The "effective" emissions $\overline{E}_k^{\text{eff}}$ in the CTM mass balance equations are reconstructed by rescaling the emissions by the ECF evaluated at the plume lifetime t_p:

$$\overline{E}_k^{\text{eff}} = \text{ECF}_k(t_p)\overline{E}_k \,. \tag{43}$$

4.3 Plume Transformation Indices (PTI) and Effective Perturbation Indices (EPI)

In the methodology proposed by Karol et al. (2000) the effective emission index is decomposed in two factors: the usual emission index that quantifies the in-engine processes (EI) and the dimensionless Plume Transformation Index (PTI):

$$\text{EEI}_k = \text{EI}_k \times \text{PTI}_k \tag{44}$$

This method follows the idea of Petry et al. (1998) of modifying the emission indices but it represents the variation of the total mass (or the number of molecules) of species by an integration over the entire plume lifetime rather than an evaluation at t_p as in the ECF method by Meijer (2001). Subtracting Eq. (15) from Eq. (14) and integrating over t_p yields after some algebra to:

$$\Delta m_k^*(t_p) = \int_{t_0}^{t_p} V_p(t)\left[\omega_k^p(t) - \omega_k^a(t)\right] dt = m_k^*(t_p) - m_k^*(t_0) \tag{45}$$

where Eq. (40) has been used. For emitted species k_e the PTI is defined as

$$\text{PTI}_{k_e}(t_0, t_p) = \frac{V_p(t_0)c_{k_e}^p(t_0) + \Delta m_{k_e}^*(t_p)}{V_p(t_0)c_{k_e}^p(t_0)} \tag{46}$$

GMDD
4, 137–196, 2011

while for species k_{ne} not emitted by the aircraft and originating in plume from interaction with the emitted species k_e, the PTI is given by

$$\mathrm{PTI}_{k_{ne}}(t_0, t_p) = \frac{m^*_{k_{ne}}(t_p)}{V_p(t_0) c^p_{k_{ne}}(t_0)}. \quad (47)$$

The plume model developed by Karol et al. (1997) was used to get the PTI_k. The chemistry scheme included 85 gas phase reactions and 33 compounds without heterogeneous chemistry. The plume simulations took place in the 9–12-km layer at 50° and 30° N in the upper troposphere and lower stratosphere inside and outside the NAFC, in January and July. The calculations of PTI confirmed the conclusions given by Meijer et al. (1997) and Petry et al. (1998) that a significant part of NO_x components emitted by subsonic aircraft may be transformed into the NO_y components in the plume stage, and that these transformations are mostly sensitive to ambient air composition (see for example Fig. 16). In particular, Karol et al. (2000) observed that flying in the warm stratosphere and out of flight corridor should reduce the released NO_x entering into large-scale and the global reservoir of the aircraft NO_y.

Meilinger et al. (2005) developed a detailed plume model to analyze the microphysical processes and heterogeneous chemistry in aircraft plumes, including the formation of persitent contrails. For emitted species, they used the definition of PTI in Eq. (46) while for non emitted species, they introduced a slightly different definition, named Effective Perturbation Index:

$$\mathrm{EPI}_{k_{ne}} = \frac{c^p_{k_{ne}}(t_{enc}) - c^a_{k_{ne}}(t_{enc})}{c^a_{k_{ne}}(t_{enc})} \quad (48)$$

where t_{enc} is the average plume encounter time in the NAFC (see Sect. 3.2.1). The simulations confirmed the high sensitivity of NO_x conversion and ozone formation/depletion on meteorological conditions, including relative humidity which affects the persistence of contrails (see Fig. 17).

GMDD
4, 137–196, 2011

The "effective" emissions $\overline{E}_k^{\text{eff}}$ in the CTM mass balance equations are reconstructed using Eqs. (8), (44) and (46)–(47)

$$\overline{E}_k^{\text{eff}} = \text{EI}_k \text{PTI}_k \left(t_0, t_\text{p}\right) \overline{S}_\text{f} \,. \tag{49}$$

4.4 Effective Reaction Rates (ERR)

The method of effective reaction rates (ERR) was introduced by Cariolle et al. (2009) to study the impact of NO_x emissions on the atmospheric ozone. The basic idea of the method is that the chemical transformations in the plume proceed with different rates than in the background atmosphere because of the high concentrations of exhausts within the plume. It is then possible to define "effective" reaction rate constants working on the fraction of the emissions within the plume (undiluted fraction). To discriminate between diluted and undiluted fractions of emissions, an additional transport equation for a fuel tracer is solved by the CTM:

$$\frac{D\overline{C}_\text{f}}{Dt} = \overline{S}_\text{f} - \frac{\overline{C}_\text{f}}{\tau} \tag{50}$$

where the last term in the right-hand side is a model for the (large-scale) fuel dilution. The decay time τ is obtained by approximating the evolution of excess of exhaust mass m_p^* in Eq. (30) by an exponential fit: $m_\text{p}^*(t) = m_\text{p}^*(t_0)\exp(-(t-t_0)/\tau)$ so that

$$\tau \equiv \int_{t_0}^{+\infty} \text{e}^{-(t-t_0)/\tau} dt = \frac{1}{m_\text{p}^*(t_0)} \int_{t_0}^{t_\text{p}} m_\text{p}^*(t) dt \tag{51}$$

where $t_\text{p} = t_\text{lim}$ is defined according to the threshold value c_lim as explained in Sect. 3.2.1. The (grid-averaged) undiluted fraction of NO_x (exhaust NO_x) is reconstructed using $\overline{C}_\text{f}$ as

$$\overline{C}_{\text{NO}_x}^\text{p} = \alpha_{\text{NO}_x} \text{EI}_{\text{NO}_x} \overline{C}_\text{f} \tag{52}$$

GMDD
4, 137–196, 2011

where $\alpha_{NO_x}=10^{-3}W_{air}/W_{NO_x}$ is a scaling factor with W_{air} and W_{NO_x} the molecular weights of air and NO_x, respectively.

To account for the effects of highly concentrated exhaust NO_x on ozone concentration, an "effective" reaction rate is introduced as:

$$\overline{K}^{\mathrm{eff}}_{NO_xO_3} = \frac{\int_{t_0}^{t_p}\left(\int_{V_p} K_{NO_xO_3} c_{NO_x} c_{O_3} dV_p\right) dt}{c^a_{O_3}\int_{t_0}^{t_p}\left(\int_{V_p} c_{NO_x} dV_p\right) dt} \quad (53)$$

where the plume concentrations can be obtained using any of the plume models introduced in Sect. 3 or explicit three-dimensional LES. The ozone balance equation in the CTM is modified by adding a term which represents the destruction of ozone by NO_x at the scale of the grid-box and proceeds at the rate $\overline{K}^{\mathrm{eff}}_{NO_xO_3}$:

$$\frac{D\overline{C}_{O_3}}{Dt} = \overline{\omega}_{O_3}(\overline{C}_1,\ldots,\overline{C}_{N_s}) - \overline{K}^{\mathrm{eff}}_{NO_xO_3}\overline{C}^{\mathrm{p}}_{NO_x}\overline{C_{O_3}}\,. \quad (54)$$

This approach is slightly different from the general formulation of effective reactions introduced in Eq. (12) in the sense that $\overline{K}^{\mathrm{eff}}_{NO_xO_3}$ is constructed in such a way that the grid-averaged undiluted fraction $\overline{C}^{\mathrm{p}}_{NO_x}$ rather than the total grid-averaged concentration $\overline{C}_{NO_x}$ appear explicitly in the ozone balance equation. The EER method gives a framework that is fully conservative for the injected species, and that relaxes to ID model when $\tau\rightarrow 0$. It was found that the NO_x-ozone chemistry inside the plume is characterized by a first regime during which NO and NO_2 get to equilibrium while ozone decreases by titration of NO_2, and by a following slower decrease of odd oxygen NO_2+O_3 species (see Fig. 18). Cariolle et al. (2009) further discuss the determination

GMDD
4, 137–196, 2011

of $\overline{K}^{\text{eff}}_{NO_xO_3}$ for ozone and the values of t_p and τ, and introduce additional terms to account for O_3 titration and the formation of nitric acid during the plume dilution.

5 Integration of emission parameterizations into global models

This section describes the results of the implementation of the different parameterizations presented in Sect. 4 into global and regional models. In order to evaluate the effects of plume processes, three baseline computations can be designed:

- run *A*: with the unmodified emission inventories for NO_x and other exhaust species
- run *B*: with the modified emissions $\overline{E}^{\text{eff}}_k$ or reaction rates $\overline{K}^{\text{eff}}_j$
- run *C*: without emissions

The perturbations due to the chemical conversions are then quantified in absolute numbers:

$$\varepsilon_k = \overline{C}_k(\text{run } A) - \overline{C}_k(\text{run } B) \tag{55}$$

and relative numbers:

$$\varepsilon_{k_{\%}} = \frac{\overline{C}_k(\text{run } A) - \overline{C}_k(\text{run } B)}{\overline{C}_k(\text{run } B) - \overline{C}_k(\text{run } C)} \times 100\,. \tag{56}$$

5.1 Application of ECF and EEI

The ECF were first implemented by Meijer et al. (1997) in the Chemistry Transport Model CTMK (Velders et al., 1994; Wauben et al., 1997) and successively by Meijer (2001) in the TM3 model (Meijer et al., 2000). The original engine exit emissions from

GMDD
4, 137–196, 2011

the DLR/ANCAT 2 NO_x emissions (Gardner et al., 1997) were transformed into aircraft plume emissions using the ECF in Eq. (43) at each computational cell. The plume lifetime was taken t_p=15 h (Meijer, 2001).

Figure 19 shows the monthly mean of absolute and relative NO_x and O_3 perturbations. As expected, the main NO_x perturbations were along the main aircraft routes, with mean values of 50–100 pptv in January, and 50–110 pptv in July in the case of unmodified ANCAT emissions. The O_3 perturbations around and in the main flight corridors were in the range of 1.8–2.1 ppbv for January and 2–3.8 ppbv for July. When the ECF parameterization was included NO_x perturbations were reduced by 15–30 pptv in January, and by 10–35 pptv in July (in relative numbers, these reductions amount to 20–30% and 20–40%, respectively). Generally, the ozone perturbation is reduced due to the efficient conversion of NO_x in the aircraft plumes, leading to a diminished O_3 production on the global scale. On the other hand, the photochemistry in the aircraft exhaust plumes generally produces additional ozone emissions. If photochemical activity is sufficiently high, net ozone production in the aircraft plumes can be large enough to enhance the aircraft-induced ozone perturbation. This explains the increase (negative reduction) of the local perturbation of ozone in the NAFC for July. The maximal enhancement was 8% (note that the results presented by Meijer (2001) are slightly different from those of Meijer et al. (1997) because the net ozone production and the time of emission had not been taken into account).

Kraabøl et al. (2000a) implemented the ECF methodology into NILU-CTM, a three-dimensional chemistry transport meso-scale model covering Europe, North America, and the North Atlantic (Flatøy et al., 1995; Simpson, 1992; Strand and Hov, 1994). The spatial distribution of aircraft NO_x emissions were taken from the DLR/ANCAT 2 (Gardner et al., 1997). The plume lifetime for the implementation of ECF was taken t_p=15 h, which, in this case, also corresponds to a plume width of approximately the size of the computational cell. Without plume modifications, the monthly averaged increases for July for NO_x and ozone were up to 70 ppt and 2.7 ppb, respectively. On the other hand, with plume modifications, the corresponding NO_x and ozone increases

GMDD
4, 137–196, 2011

were reduced by 30 ppt (~40%) and 0.5 ppb (~20%), respectively (see Fig. 20). The ozone increase within the North Atlantic Flight Corridor (NAFC) was also reduced by up to 0.5 ppb (~30%).

Kraabøl et al. (2002) implemented the plume model into the OSLO-CTM2 (Sundet, 1997), which is based on the chemical scheme described by Hesstvedt et al. (1978) and Berntsen and Isaksen (1999). The implementation of ECF is very similar to that used by Kraabøl et al. (2000a), expect that the variations in the turbulent conditions of the atmosphere were taken into account: following Dürbeck and Gerz (1996), the diffusivities needed by the plume model, Eqs. (16)–(18), where reconstructed in each computational cell using the probability density function of Brunt-Väisälä frequency N and vertical wind shear s from the ECMWF forecast data in the Northern Hemisphere between 8 and 12 km. Furthermore, the plume was followed until either the size was considered large enough to be representative for the grid resolution of OSLO-CTM2 or the NO_x emissions were homogeneously mixed with the surrounding air, i.e. t_p=MIN(t_{ref}, t_{mix}), see Eq. (28) (a value of 48 h was taken as an upper limit).

When plume modifications with variable turbulence are included in the global model, the aircraft-induced NO_x and ozone increases in the NAFC and over Europe were reduced (see Fig. 21). The absolute (relative) reductions were strongest in April/May, where NO_x and ozone decreased by 15 to 25 pptv (25–35%) and 0.8 to 1 ppbv (15–18%) at northern midlatitudes, respectively. The corresponding numbers were estimated to 8 to 22 ppt (20%) for NO_x and 0.4 to 0.6 ppb (15–20%) for ozone in January. Kraabøl et al. (2002) finally pointed out a few issues on the modeling of ECF of NO_x that deserve further investigation. The first issue concerns the assumption of stationary turbulence during the plume lifetime: for certain (weak) values of N and s from ECMWF data, this may overestimate the dispersion time of the plume to reach the resolved scale of the global model. In real atmosphere, the plume is likely to encounter conditions that favor much higher dispersion over that period. In this case the ozone production efficiency will be higher than that predicted by the simulations. The second issue is that the emissions were represented as a single plume, whereas in reality, the

GMDD
4, 137–196, 2011

emissions within a computational cell of a CTM consist of multiple plumes. Mixing of multiple plumes causes a lower fraction of the emitted NO_x to be converted into NO_y in the plume (Kraabøl et al., 2002). Thus, more NO_x will remain as NO_x when the plume reaches the resolved scale of the CTM. This will lead to a higher ozone production efficiency of emissions.

The EEI and ECF techniques were recently tested by Vohralik et al. (2008) using the same plume model and the CSIRO two-dimensional chemical transport model (Randeniya et al., 2002). The comparison between the two techniques showed significant differences in the predicted NO_x increase although the aircraft-induced ozone perturbations were found relatively small. In general, the predicted effects on the global impact of ozone were comparable in magnitude to those found by Meijer (2001) but considerably smaller than those obtained by Kraabøl et al. (2002).

5.2 Application of ERR

The ERR method (Cariolle et al., 2009) has been implemented in the 3-D model LMDz-INCA (Hauglustaine et al., 2004; Folberth et al., 2006) coupled to the AERO2K emission database (Eyers et al., 2004). Figure 22 shows that the large-scale NO_x content decreases significantly over the main flight corridors due to their storage in high-concentration plume form and to the conversion of a fraction of the NO_x into HNO_3. This large scale NO_x decrease reduces the background O_3 production that adds to the direct local O_3 destruction found within the plume air masses. The result is a reduction of the global aircraft induced O_3 production by about 15% in the Northern Hemisphere when the plume effects are taken into account. This result is consistent with the evaluations made using the EEI and ECF methods.

The ERR method has been recently adapted by Huszar et al. (2010) to treat the case of NO_x emissions by ships within the near Atlantic European Corridor. The simulations were carried out using the CAMX, an Eulerian photochemical dispersion model developed by ENVIRON Int. Corp. (http://www.camx.com) coupled to the

GMDD
4, 137–196, 2011

UNECE/EMEP emission database for year 2003 (Vestreng et al., 2007). Model results show that the ship traffic emissions strongly modify NO_x levels not only over remote ocean but also at coastal areas and to some extent over land at greater distances from the sea. Highest levels of 4–6 ppbv are found over the English Channel during both seasons with peaks up to 8 ppbv in summer. With the inclusion of the ERR plume parameterization (with t_p=1 h), the average surface large-scale NO_x concentration decreases by up to 0.1 ppbv over remote sea during both seasons. The reduction in the main corridors is much stronger and exceeds 1 ppbv at peak levels in both summer and winter (see Fig. 23). This can be also interpreted as the modification of the NO_x perturbation caused by ship emissions. In relative numbers, model simulations show that ship NO_x perturbation is reduced by more than 10% along shipping routes. Areas of intensive ship traffic (coastal regions and the most important shipping corridors) indicate larger reduction up to 20–25%. As a consequence, ozone production due to the ship emission is reduced and the level of ozone decreases both in summer and winter seasons. The reduction occurs on the whole area of the European domain with the largest effects in the shipping corridors where the ozone reduction reaches values of about 0.4–0.7 ppbv in winter and 1–2 ppbv during summer conditions.

6 Conclusions

This study presented a summary of various methods proposed in the literature to parameterize the chemical transformations of emissions from concentrated sources into large-scale models. All the analyzed parameterizations are based on a two-step procedure: first a data-set from a small-scale model is generated; then these data are transfered to the global model. The data-set can be obtained using single plume models with various levels of sophistication, or even large-eddy simulations, depending on the accuracy required to represent plume processes. However, the choice of the data that are to be transferred and the way they are incorporated in the global models vary substantially among the different parameterizations. These differences are now briefly discussed.

GMDD
4, 137–196, 2011

In the EEI and the ECF/PTI methods, the emission rates themselves are modified, i.e., the source terms E_k in Eq. (8) are rescaled by some factors that take into account the chemical transformations in the plume. In the EEI method, the correction is directly made at emission time by changing the original emission index EI "as if" an equivalent emission were instantaneously dispersed at large scale, see Fig. (8). On the other hand, in the ECF method the emissions are rescaled by the excess of concentrations over background at the end of the plume lifetime $t=t_p$ as shown in Fig. (12). It is worth observing that if the large-scale transport is switched off (steady state or $D/Dt=0$), the two methods should provide the same results at $t=t_p$ since the species concentrations are determined by the same plume model. Note that since the concentration emissions are changed, additional corrections are needed in both methods to insure conservation (respectively a minimization procedure, Eq. 34 in EEI method, and a re-normalization by the NO_y excess in the ECF method).

In the ERR method, the reaction rates rather than the emissions themselves are modified which automatically insure conservation. In the case of secondary formed species like ozone, the use of effective reaction rates does not directly introduce pre-computed tendencies, but act as a modulation of the chemical cycles existing in the background atmosphere. Furthermore, the method takes into account the transport of pollutants during the plume dilution by explicitly solving a transport equation for fuel tracer. Thus, the non-linear chemical effects can apply rather far from the point of injection depending on the large-scale advection and the plume lifetime. This also insure that EER relaxes to the ID model as $\tau \rightarrow 0$. Nevertheless, the ERR method still requires that some key reactions within the plume have to be identified in order to compute the relevant effective reactions.

The implementation of methods described here require that a good consistency exits between the chemical processes represented in the plume and in the background atmosphere. This consistency can be easily insured for gas phase chemistry, but it is more difficult to achieve for heterogeneous processes because of the different level of complexity used to represent them in plume models and the 3-D large-scale

GMDD
4, 137–196, 2011

models. In the case of aircraft emissions, this is particularly important when under specific atmospheric conditions long-lasting contrails transform into cirrus clouds. In those cases, the microphysics used in the plume model has to be consistent with the cloud parameterization of the large scale model.

Acknowledgements. This work was supported by the European Union FP6 Integrated Project QUANTIFY (http://www.pa.op.dlr.de/quantify/).

The publication of this article is financed by CNRS-INSU.

References

Berntsen, T. K. and Isaksen, I. S. A.: The effect of lightning and convection on changes in tropospheric ozone due to NO_x emissions from aircraft, Tellus B, 51, 766–788, 1999. 161

Brasseur, G. P., Müller, J.-F., and Granier, C.: Atmospheric impact of NO_x emissions by subsonic aircraft, J. Geophys. Res., 101, 1423–1428, 1996. 139

Brasseur, G. P., Cox, R. A., Hauglustaine, D., Isaksen, I., Lelieveld, J., Lister, D. H., Sausen, R., Schumann, U., Wahner, A., and Wiesen, P.: European scientific assessment of the atmospheric effects of aircraft emissions, Atmos. Environ., 32, 2329–2418, 1998. 138

Cariolle, D., Caro, D., Paoli, R., Hauglustaine, D., Cuenot, B., Cozic, A., and Paugam, R.: Parameterization of plume chemistry into large scale atmospheric models: application to aircraft NO_x emissions, J. Geophys. Res., 114, D19302, doi:10.1029/2009JD011873, 2009. 139, 149, 150, 157, 158, 162, 179, 191, 195

GMDD

4, 137–196, 2011

Cess, R. D., Potter, G. L., Blanchet, J. P., Boer, G. J., Del, G., Deque, M., Dymnikov, V., Galin, V., Gates, W.-L., Ghan, S. J., Kiehi, J. T., Lacis, A. A., Le, T.-H., Li, Z. X., Liang, X. Z., McAvaney, B. J., Meleshko, V. P., Mitchell, J. F. B., Morcrette, J. J., Randall, D. A., Rikus, L., Roeckner, E., Royer, J.-F., Schlese, U., Sheinin, D. A., Slingo, A., Sokolov, A. P., Taylor, K. E., Washington, W. M., Wetherald, R. T., Yagai, I., and Zhange, M. H.: Intercomparison and interpretation of climate feedback processes in 19 atmospheric general circulation models, J. Geophys. Res., 95, 16601–16615, 1990. 138

Chosson, F., Paoli, R., and Cuenot, B.: Ship plume dispersion rates in convective boundary layers for chemistry models, Atmos. Chem. Phys., 8, 4841–4853, doi:10.5194/acp-8-4841-2008, 2008. 144

Danilin, Y. M., Rodriguez, J. M., Ko, M. K. W., Weisenstein, D. K., Brown, R. C., Myake-Lye, R., and Anderson, M. R.: Evolution of the concentrations of trace species in an aircraft plume: trajectory studies, J. Geophys. Res., 99, 18951–18972, 1994. 139

De More, W. B., Sander, S. P., Golden, D. M., Molina, M. J., Hampson, R. F., Kuyko, M. J., Howard, C. J., Ravishankara, A. R., and Kolb, C. E.: Chemical kinetics and photochemical data for use in stratospheric modeling. Evalutaion number 12, Tech. Rep., Publ. 97-4, JPL, 1997. 154

Dürbeck, T. and Gerz, T.: Dispersion of aircraft exhausts in the free atmosphere, J. Geophys. Res., 101, 26007–26016, 1996. 161

Durkee, P. A., Chartier, R. E., Brown, A., Trehubenko, E. J., Rogerson, S. D., Skupniewicz, C., Nielsen, K. E., Platnick, S., and King, M. D.: Composite ship track characteristics, J. Atmos. Sci., 57, 2542–2553, 2000. 147

Eyers, C. J., Norman, P., Middel, J., Plohr, M., Atkinson, K., and Christou, R. A.: AERO2k global aviation emissions inventories for 2002 and 2025, Tech. Rep. QINETIQ/04/01113, QINETIQ, available at: http://www.cate.mmu.ac.uk/reports_aero2k.asp?chg=projects&chg2+2, 2004. 162

Eyring, V., Stevenson, D. S., Lauer, A., Dentener, F. J., Butler, T., Collins, W. J., Ellingsen, K., Gauss, M., Hauglustaine, D. A., Isaksen, I. S. A., Lawrence, M. G., Richter, A., Rodriguez, J. M., Sanderson, M., Strahan, S. E., Sudo, K., Szopa, S., van Noije, T. P. C., and Wild, O.: Multi-model simulations of the impact of international shipping on Atmospheric Chemistry and Climate in 2000 and 2030, Atmos. Chem. Phys., 7, 757–780, doi:10.5194/acp-7-757-2007, 2007. 138

GMDD
4, 137–196, 2011

Flatøy, F., Hov, Ø., and Smit, H.: Three-dimensional model studies of exchange processes of ozone in the troposphere over Europe, J. Geophys. Res., 100, 11465–11481, 1995. 160
Folberth, G. A., Hauglustaine, D. A., Lathière, J., and Brocheton, F.: Interactive chemistry in the Laboratoire de Météorologie Dynamique general circulation model: model description and impact analysis of biogenic hydrocarbons on tropospheric chemistry, Atmos. Chem. Phys., 6, 2273–2319, doi:10.5194/acp-6-2273-2006, 2006. 162
Franke, K., Eyring, V., Sander, R., Hendricks, J., Laurer, A., and Sausen, R.: Toward effective emissions of ships in global models, Meteorol. Z., 17, 117–129, 2008. 139, 153, 184
Galmarini, S., Vinuesa, J.-F., and Martilli, A.: Modeling the impact of sub-grid scale emission variability on upper-air concentration, Atmos. Chem. Phys., 8, 141–158, doi:10.5194/acp-8-141-2008, 2008. 141
Gardner, R. M., Adams, K., Cook, T., Deidewig, F., Ernedal, S., Falk, R., Fleuti, E., Herms, E., Johnson, C. E., Lecht, M., Lee, D. S., Leech, M., Lister, D., Massé, B., Metcalfe, M., Newton, P., Schmitt, A., Vanderbergh, C., and van Drimmelen, R.: The ANCAT/EC global inventory of NO_x emissions from aircraft, Atmos. Environ., 31, 1751–1756, 1997. 160
Gerz, T., Dürbeck, T., and Konopka, P.: Transport and effective diffusion of aircraft emissions, J. Geophys. Res., 103, 25905–25914, 1998. 143, 174
Hanna, S. R., Schulman, L. L., Paine, R. J., Pleim, J. E., and Baer, M.: Develpment and evaluation of the offshore and coastal dispersion model, J. Air Pollut. Control Assoc., 35, 1039–1047, 1985. 147
Hass, H.: Description of the EURAD Chemistry-Transport Model Version 2 (CTM2), in: Mitteilungen, edited by: Ebel, A., Neubauer, F. M., and Speth, P., Inst. for Geophys. and Meteorol., Univ. of Køln, 1991. 152
Hauglustaine, D. A., Hourdin, F., Jourdain, L., Filiberti, M. A., Walters, S., Lamarque, J. F., and Holland, E. A.: Interactive chemistry in the Laboratoire de Météorologie Dynamique general circulation model: description and background tropospheric chemistry evaluation, J. Geophys. Res., 109, D04314, doi:10.1029/2003JD003957, 2004. 138, 162
Hesstvedt, E., Hov, Ø., and Isaksen, I. S. A.: Quasi-steady-state approximations in air pollution modelling. Comparison of two numerical schemes of oxidant prediction, Int. J. Chem. Kinetics, 10, 971–994, 1978. 161
Huszar, P., Cariolle, D., Paoli, R., Halenka, T., Belda, M., Schlager, H., Miksovsky, J., and Pisoft, P.: Modeling the regional impact of ship emissions on NO_x and ozone levels over the Eastern Atlantic and Western Europe using ship plume parameterization, Atmos. Chem. Phys., 10,

GMDD
4, 137–196, 2011

6645–6660, doi:10.5194/acp-10-6645-2010, 2010. 139, 162, 196
Jaeglé, L., Jacob, D. J., Brune, W. H., Tan, D., Faloona, I. C., Weinheimer, A. J., Ridley, B. A., Campos, T. L., and Sachse, G. W.: Sources of HO_x and ozone production in the upper troposphere over the United States, Geophys. Res. Lett., 24, 1709–1712, 1998. 139
Kärcher, B.: Heterogeneous chemistry in aircraft wakes: constraints for uptake coefficients, J. Geophys. Res., 102, 19119–19135, 1997. 154
Karol, I. L., Ozolin, Y. E., and Rozanov, E. V.: Box and Gaussian plume models of the exhaust composition evolution of subsonic transport aircraft in- and out of the flight corridor, Ann. Geophys., 15, 88–96, doi:10.1007/s00585-997-0088-0, 1997. 156
Karol, I., Ozolin, Y. E., Kiselev, A. A., and Rozanov, E. V.: Plume Transformation Index (PTI) of the subsonic aircraft exhausts and their dependence on the external conditions, Geophys. Res. Lett., 27, 373–376, 2000. 149, 155, 156
Kasibhatla, P., Levy II, H., Moxim, W. J., Pandis, S. N., Corbett, J. J., Peterson, M. C., Honrath, R. E., Frost, G. J., Knapp, K., Parrish, D. D., and Reyerson, T. B.: Do emissions from ships have a significant impact on concentrations of nitrogen oxides in the marine boundary layer?, Atmos. Environ., 37, 2663–2679, 2003. 139
Konopka, P.: Analytical Gaussian solutions for anisotropic diffusion in a linear shear flow, J. Non-Equilib. Thermodyn., 20, 78–91, 1995. 146
Kraabøl, A. G. and Stordal, F.: Modelling chemistry in aircraft plumes 2: the chemical conversion of NO_x to reservoir species under different conditions, Atmos. Environ., 34, 3951–3962, 2000. 154
Kraaøbl, A. G., Stordal, F., Konopka, P., and Knudsen, S.: The NILU aircraft plume model: a technical description, Tech. Rep. NILU TR 4/99, Norvegian Institute for Air Research, 1999. 138, 154
Kraabøl, A. G., Flatøy, F., and Stordal, F.: Impact of NO_x emissions from subsonic aircraft: Inclusion of plume processes in a three-dimensional modeling covering Europe, North America and North Atlantic, J. Geophys. Res., 105, 3573–3582, 2000a. 160, 161, 193
Kraabøl, A. G., Konopka, P., Stordal, F., and Schlager, H.: Modelling chemistry in aircraft plumes 1: comparison with observations and evaluation of a layered approach, Atmos. Environ., 34, 3939–3950, 2000b. 146, 147, 148, 149, 154, 176
Kraabøl, A. G., Berntsen, T. K., Sundet, J. K., and Stordal, F.: Impacts of NO_x emissions from subsonic aircraft in a global three-dimensional chemistry transport model including plume processes, J. Geophys. Res., 107, 4655–4667, 2002. 139, 149, 161, 162, 194

GMDD
4, 137–196, 2011

Lawrence, M. G. and Crutzen, P. J.: Influence of NO_x emissions from ships on tropospheric photochemistry and climate, Nature, 402, 167–170, 1999. 138

Lewellen, D. C. and Lewellen, W. S.: The effects of aircraft wake dynamics on contrail development, J. Atmos. Sci., 58, 390–406, 2001a. 144

Lewellen, D. C. and Lewellen, W. S.: Effects of aircraft wake dynamics on measured and simulated NO_x and HO_x wake chemistry, J. Geophy. Res., 106, 27661–27672, 2001b. 144

Lin, K., Trainer, M., and Liu, S. C.: On the nonlinearity of the tropospheric ozone production, J. Geophys. Res., 93, 15879–15888, 1998. 139

Meijer, E. W.: Modeling the impact of subsonic aviation on the composition of the atmosphere, Ph.D. thesis, Technische Universiteit Eindhoven, 2001. 147, 148, 149, 150, 153, 154, 155, 159, 160, 162, 178

Meijer, E. W., van Velthoven, P. F. J., Wauben, W. M. F., Beck, J. P., and Velders, G. J. M.: The effect of the conversion of the nitrogen oxides in aircraft exhaust plumes in global models, Geophys. Res. Lett., 24, 3013–3016, 1997. 139, 153, 156, 159, 160

Meijer, E. W., van Velthoven, P. F. J., Thompson, A. M., Pfister, L., Schlager, H., Schulte, P., and Kelder, H.: Model calculations of the impact of NO_x from air traffic, lightning, and surface emissions compared with measurements, J. Geophys. Res., 105, 3833–3850, 2000. 138, 159

Meilinger, S. K., Kärcher, B., and Peter, Th.: Microphysics and heterogeneous chemistry in aircraft plumes – high sensitivity on local meteorology and atmospheric composition, Atmos. Chem. Phys., 5, 533–545, doi:10.5194/acp-5-533-2005, 2005. 150, 156

Melo, O. T., Lusis, M. A., and Stevens, R. D. S.: Mathematical modelling of dispersion and chemical reactions in a plume – Oxidation of NO to NO_2 in the plume of a power plant, Atmos. Environ., 12, 1231–1234, 1978. 147

Paoli, R.: Modeling and simulation of the environmental impact of aircraft emissions, Habilitation à Diriger des Recherches (HDR) dissertation, Institut National Polytechnique de Toulouse, 2010. 174

Paoli, R., Hélie, J., and Poinsot, T.: Contrail formation in aircraft wakes, J. Fluid Mech., 502, 361–373, 2004. 144

Paugam, R., Paoli, R., and Cariolle, D.: Influence of vortex dynamics and atmospheric turbulence on the early evolution of a contrail, Atmos. Chem. Phys., 10, 3933–3952, doi:10.5194/acp-10-3933-2010, 2010. 144

GMDD
4, 137–196, 2011

Petry, H., Hendricks, J., Möllhoff, M., Lippert, E., Meier, A., and Sausen, R.: Chemical conversion of subsonic aircraft emissions in the dispersing plume: Calculation of effective emission indices, J. Geophys. Res., 103, 5759–5772, 1998. 139, 147, 149, 150, 151, 152, 153, 155, 156, 177, 181

Randeniya, L. K., Vohralik, P. F., and Plumb, I. C.: Stratospheric ozone depletion at northern mid latitudes in the 21st century, Geophys. Res. Lett., 29(4), 1051, doi:10.1029/2001GL014295, 2002. 162

Roeckner, E., Arpe, K., Bengtsson, L., Christoph, M., Claussen, M., Dumenil, M., Esch, M., Giorgetta, M., Schlese, U., and Schulzweida, U: The atmospheric general circulation model ECHAM-4: model description and simulation of present-day climate, Tech. Rep. 218, MPI, 1996. 138

Sander, R., Kerkweg, A., Jöckel, P., and Lelieveld, J.: Technical note: The new comprehensive atmospheric chemistry module MECCA, Atmos. Chem. Phys., 5, 445–450, doi:10.5194/acp-5-445-2005, 2005. 153

Schlager, H., Konopka, P., Schulte, P., Schumann, U., Ziereis, H., Arnold, F., Klemm, M., Hagen, D., Whitefield, P., and Ovarlez, J.: In situ observations of air traffic emission signatures in the North Atlantic flight corridor, J. Geophys. Res., 102, 10739–10750, 1997. 139

Schlager, H., Baumann, R., Lichtenstern, M., Petzold, A., Arnold, F., Seidel, M., Gurk, C., and Fischer, H.: Aircraft-based trace gas measurements in a primary European ship corridor, in: Proc. International Conference on Transport, Atmosphere and Climate, Oxford, UK, 2006. 139

Schumann, U., Konopka, P., Baumann, R., Busen, R., Gerz, T., Schlager, H., Schulte, P., and Volkert, H.: Estimate of diffusion parameters of aircraft exhaust plumes near the tropopause from nitric oxide and turbulence measurements, J. Geophys. Res., 100, 14147–14162, 1995. 146, 172

Seinfeld, J. N. and Pandis, S. N.: Atmospheric Chemistry and Physics: From Air Pollution to Climate Change, Wiley-Interscience, Hoboken, New Jersey, 2006. 147

Simpson, D.: Long-period modelling of photochemical oxidants in Europe: (A) Hydrocarbon reactivity and ozone formation in Europe, (B) On the linearity of country-to-country ozone calculations in Europe, Tech. Rep. EMEP MSC-W Note 1/92, Norway Meteorological Institute, 1992. 160

Song, C. H., Chen, G., Hanna, S. R., Crawford, J., and Davis, D. D.: Dispersion and chemical evolution of ship plumes in the marine boundary layer: investigation of $O_3/NO_x/HO_x$

GMDD
4, 137–196, 2011

chemistry, J. Geophys. Res., 108(D4), 4143, doi:10.1029/2002JD002216, 2003. 139, 147, 153
Stockwell, W. R.: A homogeneous gas phase mechanism for use in a regional acid deposition model, Atmos. Environ., 20, 1615–1632, 1986. 152
Stockwell, W. R., Middleton, P., Chang, J. S., and Tang, X.: The second generation regional acid deposition model chemical mechanism for regional air quality modeling, J. Geophys. Res., 95, 16343–16367, 1990. 152
Strand, A. and Hov, Ø.: A two-dimensional global study of tropospheric ozone production, J. Geophys. Res., 99, 22877–22895, 1994. 154, 160
Sundet, J. K.: Model studies with a 3-D global CTM using ECMWF data, Ph.D. thesis, University of Oslo, 1997. 161
Velders, G. J. M., Heijboer, L. C., and Kelder, H.: The simulation of the transport of aircraft emissions by a three-dimensional global model, Ann. Geophys., 12, 385–393, doi:10.1007/s00585-994-0385-9, 1994. 138, 159
Vestreng, V., Mareckova, K., Kakreka, S., Malchykina, A., and Kukkharchyk, T.: Inventory review 2007, Emission data reported to LRTAP Convention and NEC Directive, Stage 1 and 2 review and Review of PM Inventories in Belarus, Republic of Moldova, Russian Federation and Ukraine, Tech. Rep. EMEP MSC-W 1/2007, Norway Meteorological Institute, 2007. 163
Vilà-Guerau de Arellano, J., Talmon, A. M., and Builtjes, P. J.-H.: A chemically reactive plume model for the NO-NO_2-O_3 system, Atmos. Environ. A, 24, 2237–2246, 1990. 147
Vohralik, P. F., Randeniya, L. K., Plumb, I. C., and Baughcum, S. L.: Impacts of NO_x emissions from subsonic aircraft in a global three-dimensional chemistry transport model including plume processes, J. Geophys. Res., 113, D05312, doi:10.1029/2007JD008982, 2008. 147, 155, 162, 188
von Glasow, R., Lawrence, M. G., Sander, R., and Crutzen, P. J.: Modeling the chemical effects of ship exhaust in the cloud-free marine boundary layer, Atmos. Chem. Phys., 3, 233–250, doi:10.5194/acp-3-233-2003, 2003. 139, 147, 173, 175
Wauben, W. M. F., van Velthoven, P. F. J., and Kelder, H.: A 3-D chemistry transport model study of changes in atmospheric ozone due to aircraft NO_x emissons, Atmos. Environ., 31, 1819–1836, 1997. 159
Zeng, G. and Pyle, J. A.: Changes in tropospheric ozone between 2000 and 2100 modeled in a chemistry-climate model, Geophys. Res. Lett., 30, 1392–1395, 2003. 138

GMDD
4, 137–196, 2011

Table 1. Diffusion parameters obtained from in situ measurements (Schumann et al., 1995).

D_h ($m^2\,s^{-1}$)	D_v ($m^2\,s^{-1}$)	D_s ($m^2\,s^{-1}$)	s (s^{-1})	$\sigma_{h,0}$ (m)	$\sigma_{v,0}$ (m)	$\sigma_{s,0}$ (m)
10	0.3	1	0.004	200	50	0

GMDD
4, 137–196, 2011

Table 2. Diffusion parameters for ship plume dispersion used by von Glasow et al. (2003) (α and β are best guest values).

α	β	$\sigma_{h,0}$ (m)	$\sigma_{v,0}$ (m)
0.75	0.6	10	5

GMDD
4, 137–196, 2011

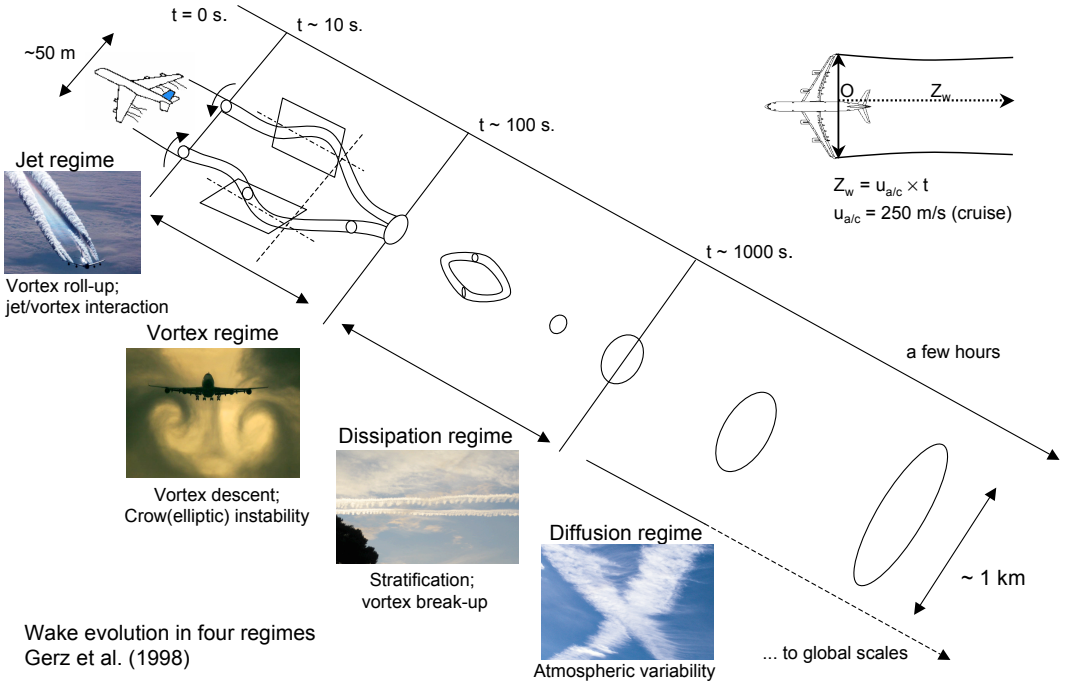

Fig. 1. Aircraft wake evolution in four regimes according to the classification made by Gerz et al. (1998). Sketch reproduced from Paoli (2010).

GMDD
4, 137–196, 2011

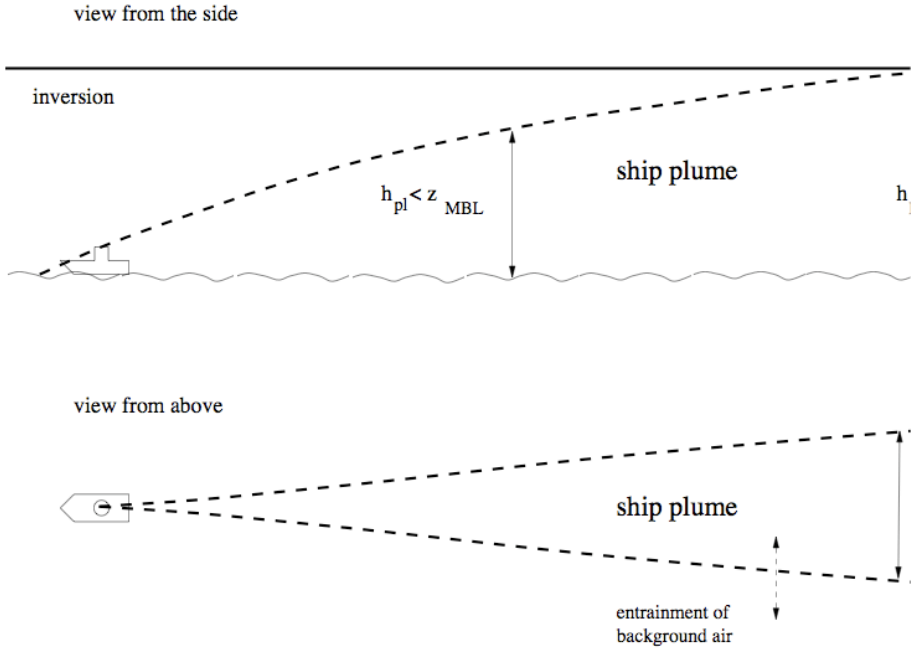

Fig. 2. Sketch of ship plume evolution in the marine boundary layer (von Glasow et al., 2003).

GMDD
4, 137–196, 2011

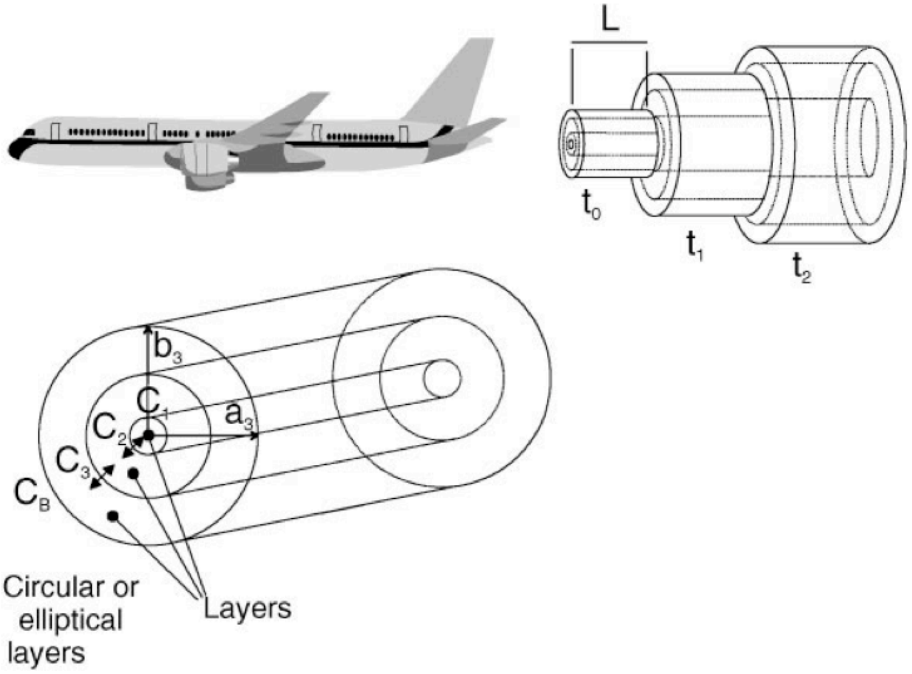

Fig. 3. Multilayer plume model of an aircraft plume (Kraabøl et al., 2000b).

GMDD
4, 137–196, 2011

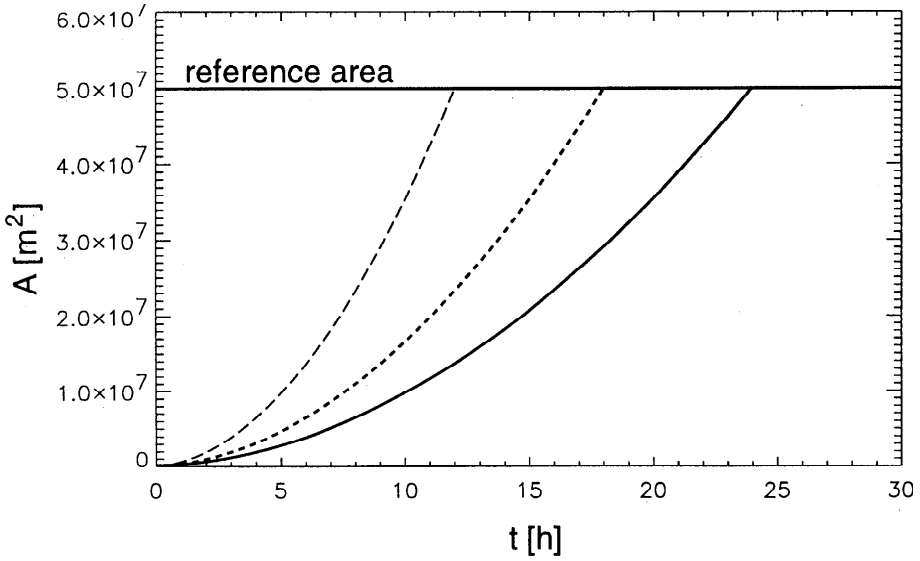

Fig. 4. Evolution of the plume cross-section A_p as a function of time; dashed line: atmospheric diffusion parameters taken from Petry et al. (1998); dotted: same but rescaled by 1.5; full: same but rescaled by 1.5. The time when A_p intersects the reference area A_{ref} defines the plume lifetime $t_p = t_{ref}$.

GMDD
4, 137–196, 2011

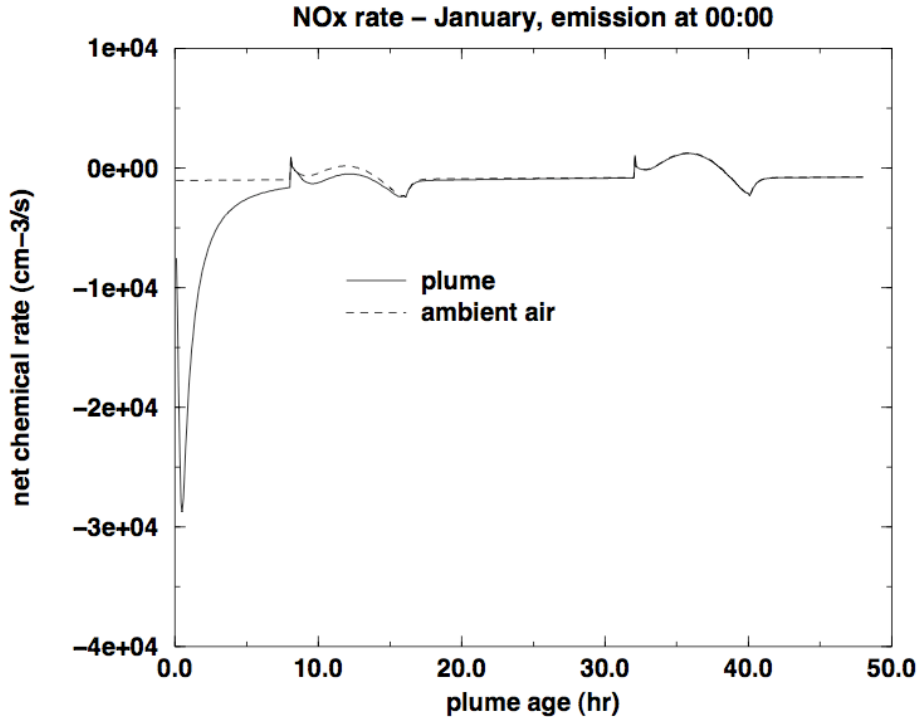

Fig. 5. Evolution of plume and background NO_x chemical rate (Meijer, 2001). The plume lifetime $t_p = t_{mix}$ is defined as the time when the difference between the two rates is below a threshold value.

GMDD
4, 137–196, 2011

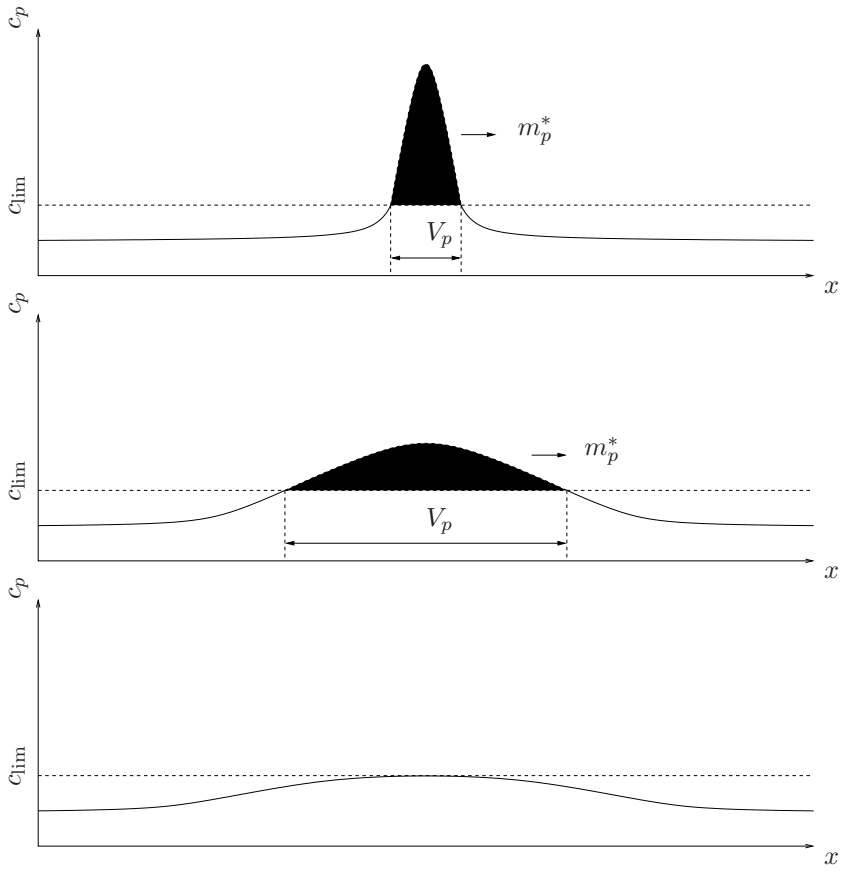

Fig. 6. Concept of plume lifetime used by Cariolle et al. (2009). Evolution of the excess of mass m_p^* over a threshold concentration c_{lim} of a chemically conserved species in the plume, from $t=t_0$ (top panel) to $t=t_{\mathrm{lim}}$ (bottom panel). The plume lifetime $t_p=t_{\mathrm{lim}}$ is defined as the time when $m_p^*=0$.

GMDD
4, 137–196, 2011

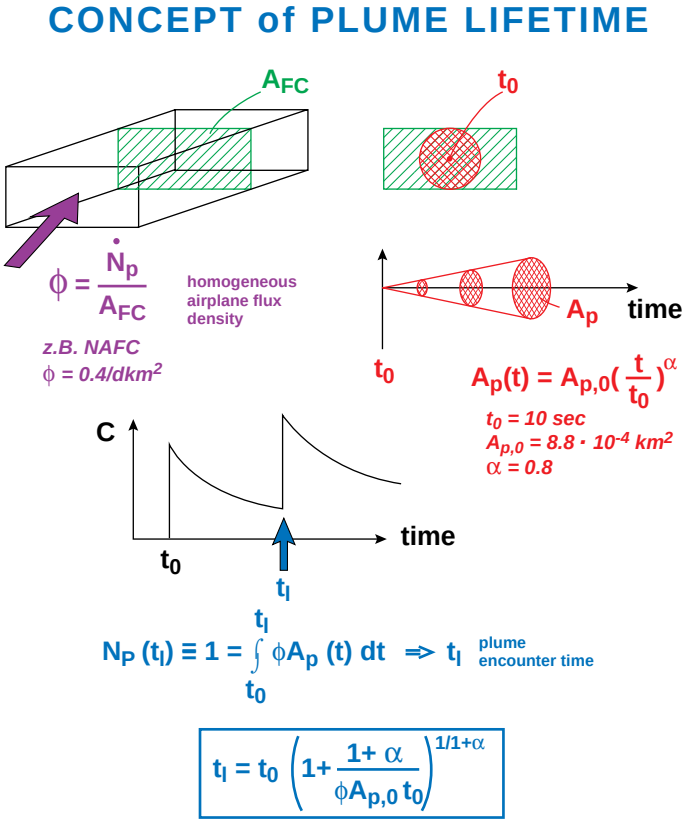

Fig. 7. Schematic description of average plume encounter time, t_{enc} of a single aircraft in a flight corridor.

GMDD
4, 137–196, 2011

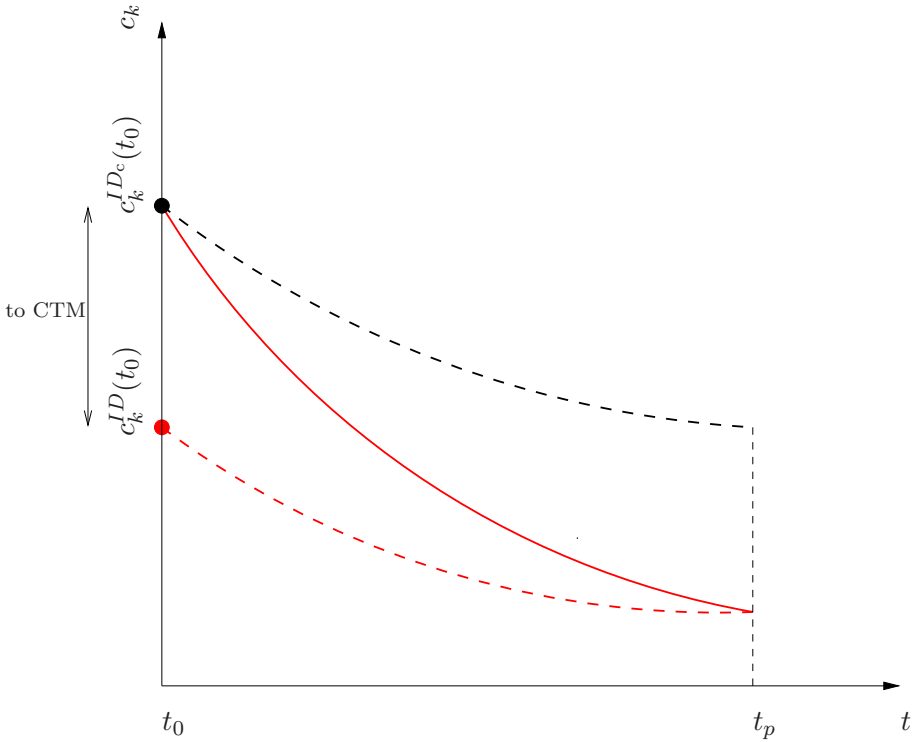

Fig. 8. Sketch of the effective emission indices (EEI) model (Petry et al., 1998). Dashed black lines: concentration evolution using the ID model with the original EI; red solid lines: concentration evolution using the SP model with the original EI; red dashed lines: concentration evolution using the ID model with the EEI.

GMDD
4, 137–196, 2011

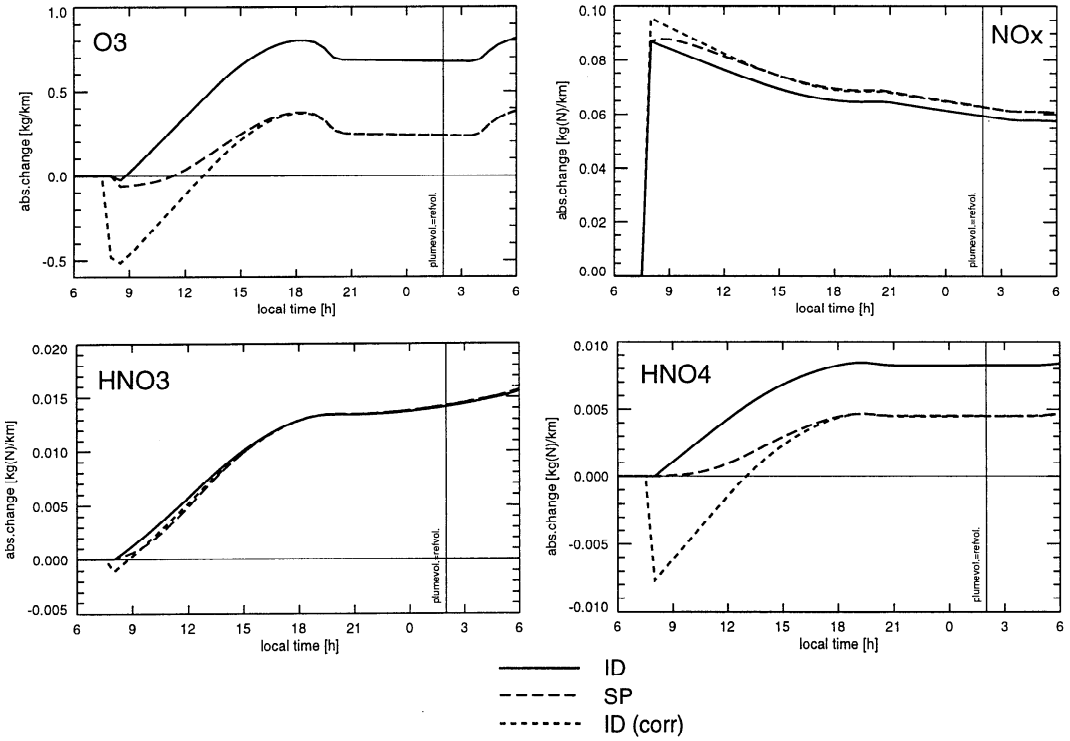

Fig. 9. Absolute changes (kg km^{-1}) of some key species caused by emission of a B-747, released at 08:00 LT into an unpolluted atmosphere (plume lifetime is τ=18 h).

GMDD
4, 137–196, 2011

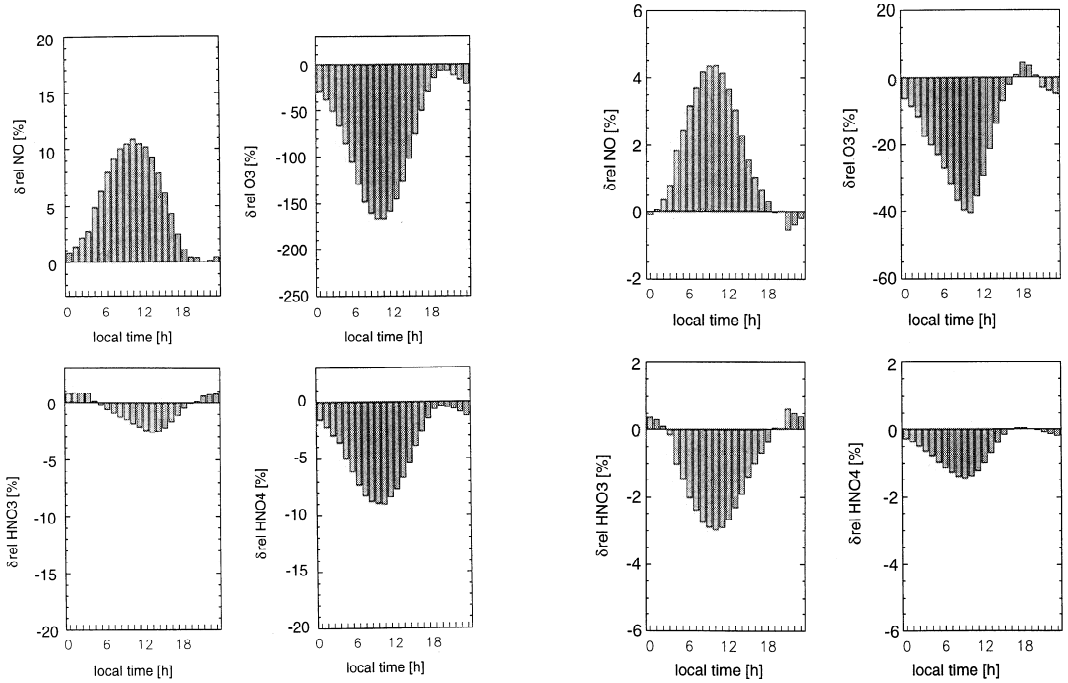

Fig. 10. Relative emission changes for calculating the effective emission indices of some key species into an unpolluted (left) and polluted (right) environment (plume lifetime is τ=18 h).

GMDD
4, 137–196, 2011

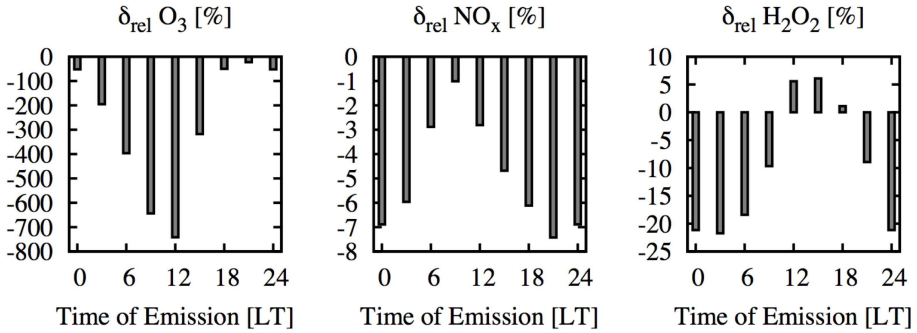

Fig. 11. Corrections of key species emissions (relative to NO_x emissions) for the calcultion of EEI from ships (Franke et al., 2008).

GMDD
4, 137–196, 2011

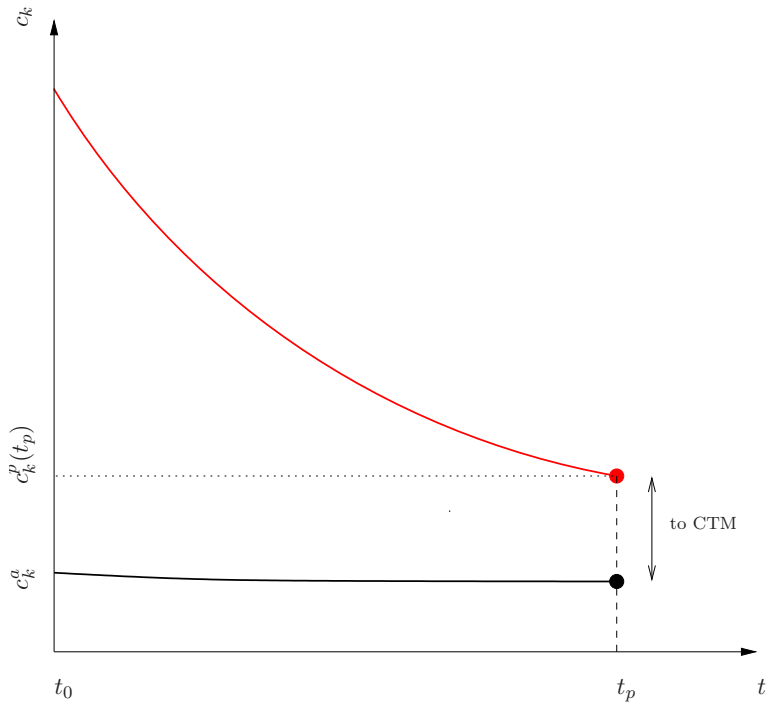

Fig. 12. Sketch of the emission conversion factor (ECF) model.

GMDD
4, 137–196, 2011

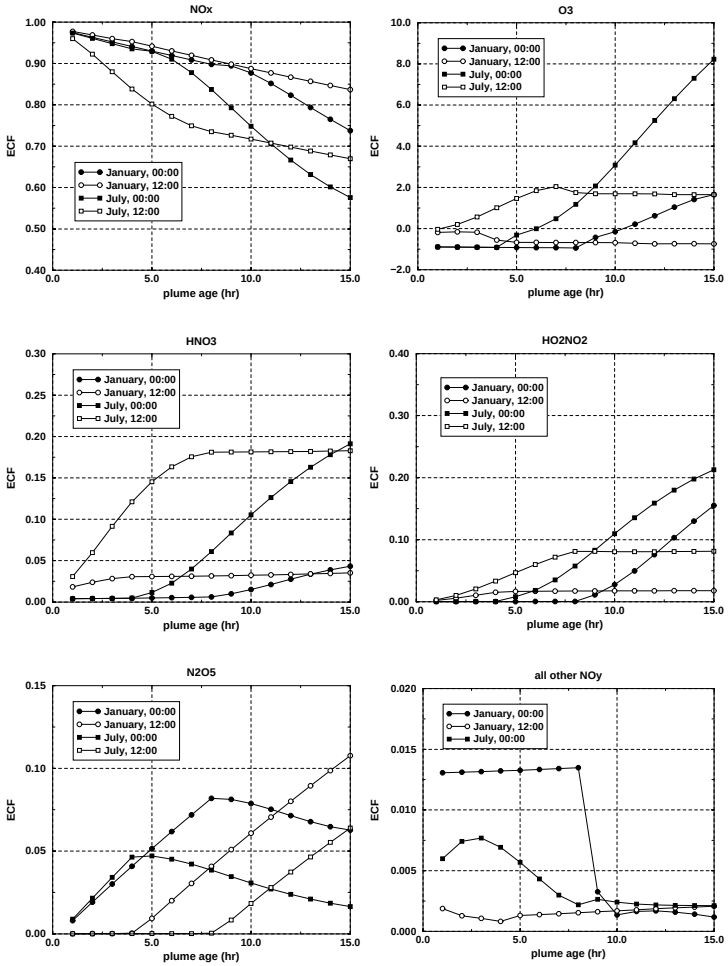

Fig. 13. Time series of emission conversion factors for some key species at different emission times.

GMDD
4, 137–196, 2011

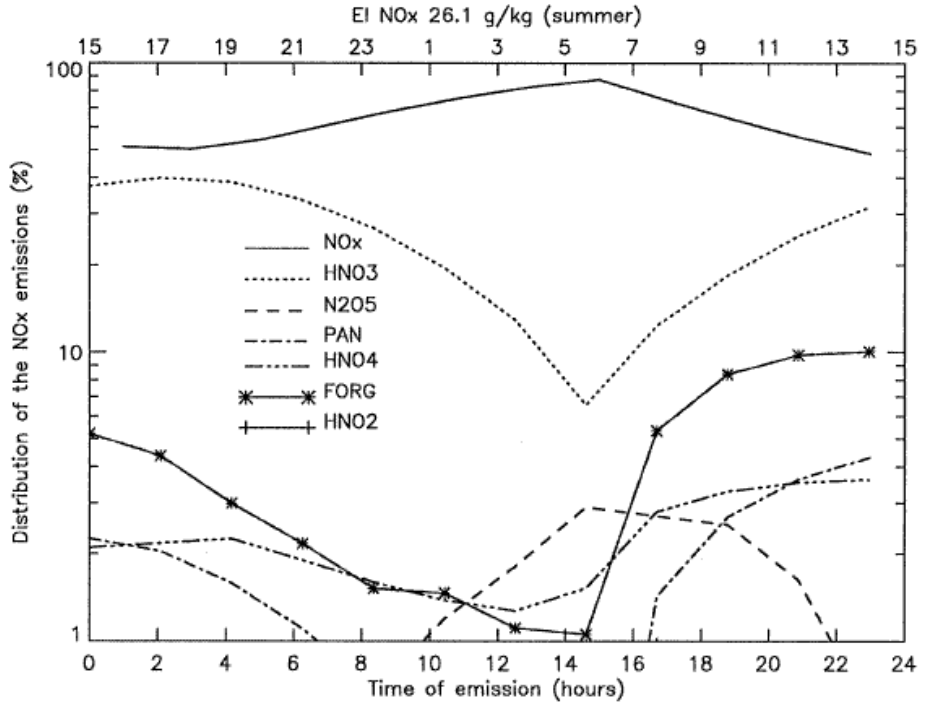

Fig. 14. Distribution of the NO_x emissions after 15 h as a function of emission time for a summer situation at 50° N. The upper axis gives the time after τ=15 h of integration. FORG=$CH_3O_2NO_2$+CH_3ONO_2+$C_2H_5ONO_2$+$C_4H_9ONO_2$ and is the sum of the oxy- and peroxynitrates included in the kinetic scheme.

GMDD
4, 137–196, 2011

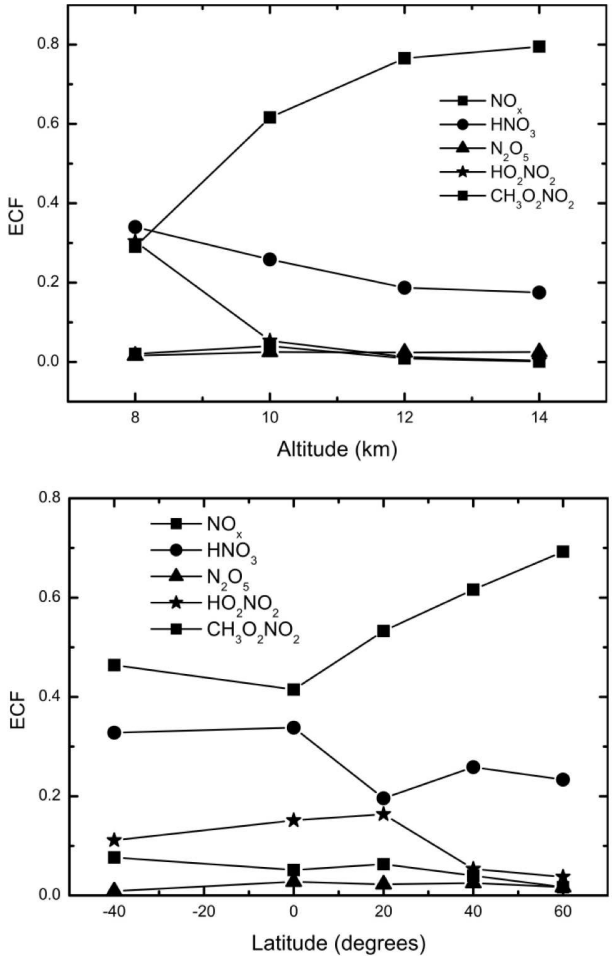

Fig. 15. Emission Conversion Factors for NO_y species computed by Vohralik et al. (2008) 24 h after emission (emission time 08:00 LT) as functions of altitude (top panel) and latitude (bottom panel).

GMDD
4, 137–196, 2011

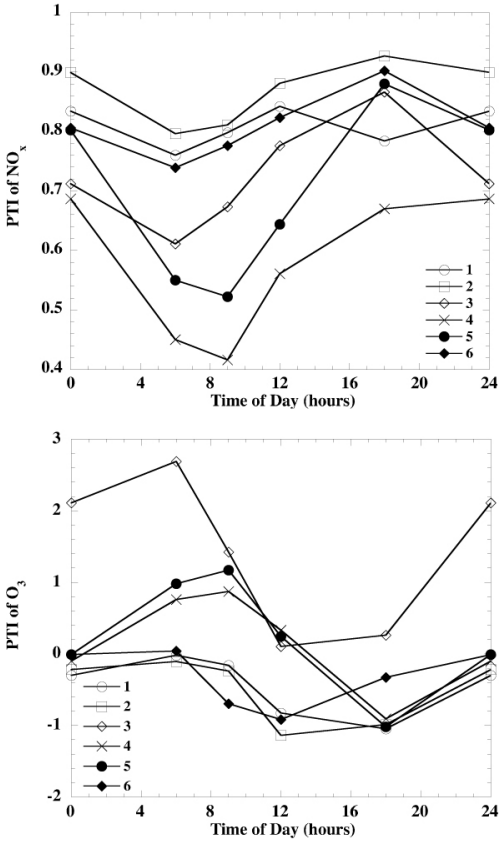

Fig. 16. Diurnal variations of PTI_{NO_x} (top panel) and PTI_{O_3} (bottom panel) in July at 50° N for different conditions: 1: lower stratosphere, inside NAFC, $T = 222$ K, P plume; 2: upper troposphere, inside NAFC, $T = 222$ K, P plume; 3: upper troposphere, outside NAFC, $T = 222$ K, P plume; 4: lower stratosphere, inside NAFC, $T = 233$ K, P plume; 5: upper troposphere, inside NAFC, $T = 233$ K, P plume; 6: upper troposphere, inside NAFC, $T = 233$ K, S plume.

GMDD
4, 137–196, 2011

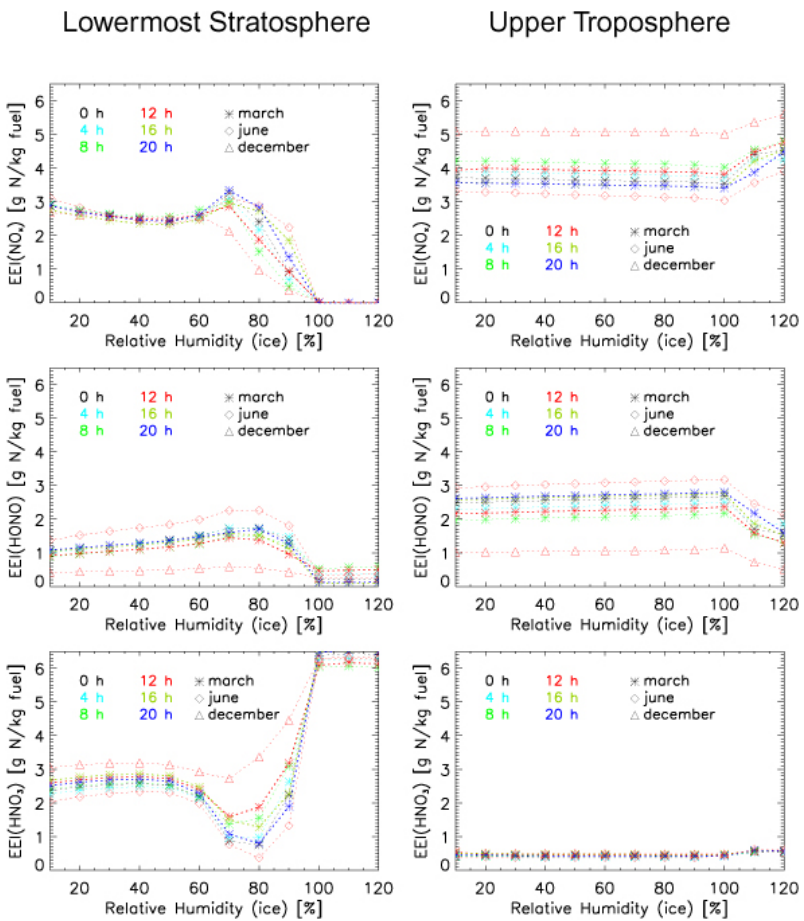

Fig. 17. Plume Transformation Indices for the NAFC ($t_l = 46$ h) as a function of RH_{ice}. Top panel: EEI_{NO_x}; middle panel: EEI_{HONO}; lower panel: EEI_{HNO_3}. The different colors and symbols show results for different local times and seasons of emission as indicated. Left: emissions into the lowermost stratosphere; right: emissions into the upper troposphere.

GMDD
4, 137–196, 2011

Modeling and computation of effective emissions

R. Paoli et al.

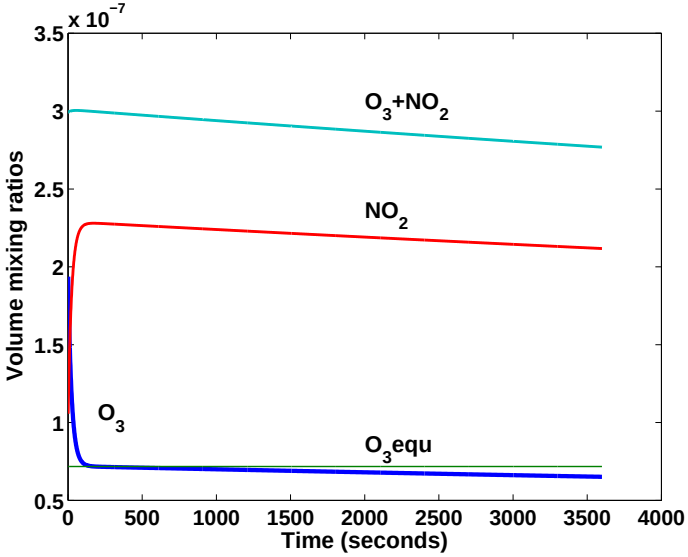

Fig. 18. Evolution of the mixing ratios of NO_x and O_3 after injection of 1 ppmv of NO_x at 200 hPa (initial conditions for the simulation: 0.2 ppmv for O_3 and $T = 230$ K). The O_3 concentration decreases rapidly due to titration by NO_2. The odd oxygen species (O_3+NO_2) show a slower continuous decrease (Cariolle et al., 2009).

GMDD
4, 137–196, 2011

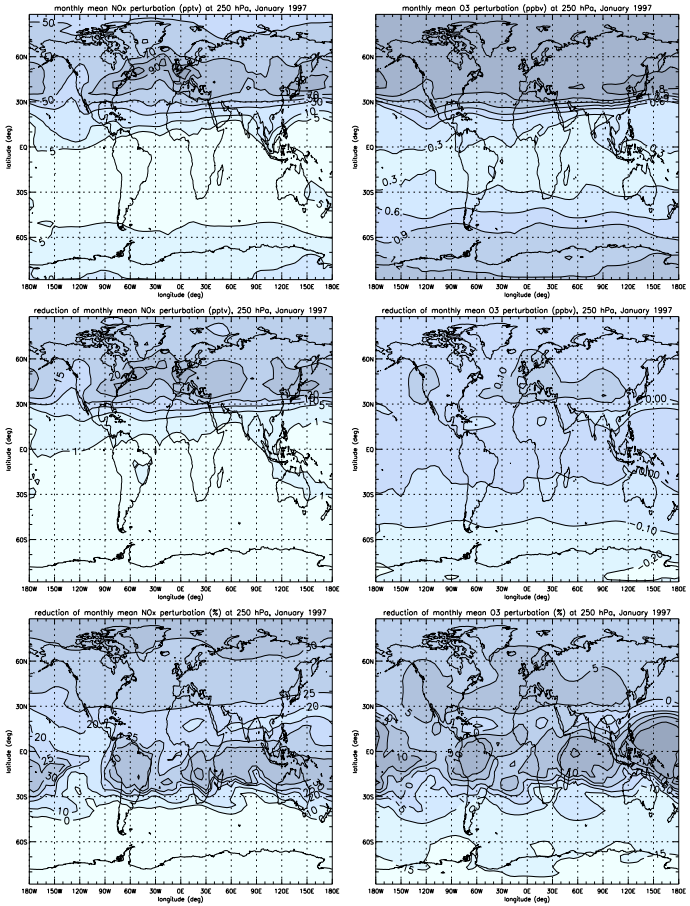

Fig. 19. Impact of aircraft NO_x on the monthly mean concentration of NO_x and O_3 at 250 hPa for January. Top panels, aircraft perturbations with no plume model (run *A*); middle panels, perturbations using ECFs (run *B*); bottom panels, percentage difference. Positive numbers in the lower four panels indicate a reduction due to the inclusion of aircraft plume emissions.

GMDD
4, 137–196, 2011

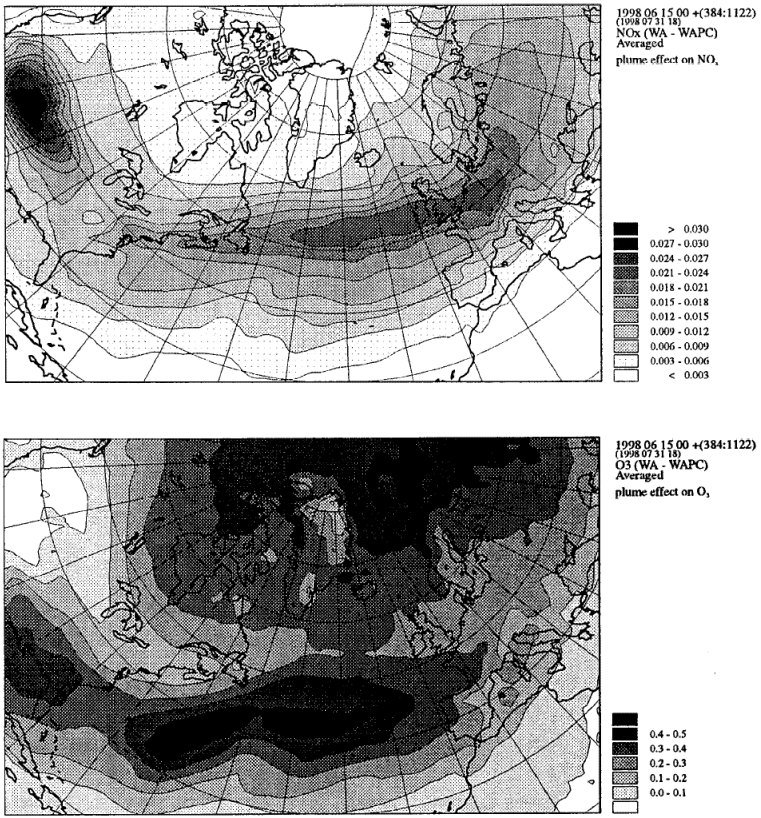

Fig. 20. Reduction in the aircraft contribution to NO_x (top) and ozone (bottom) due to plume processes in the NAFC. All numbers are in ppb. The results shown are from level four, counting from the 100 hPa model top, σ-coordinates are used and the height of the level equals 215 hPa when the ground pressure is 1000 hPa (Kraabøl et al., 2000a).

GMDD
4, 137–196, 2011

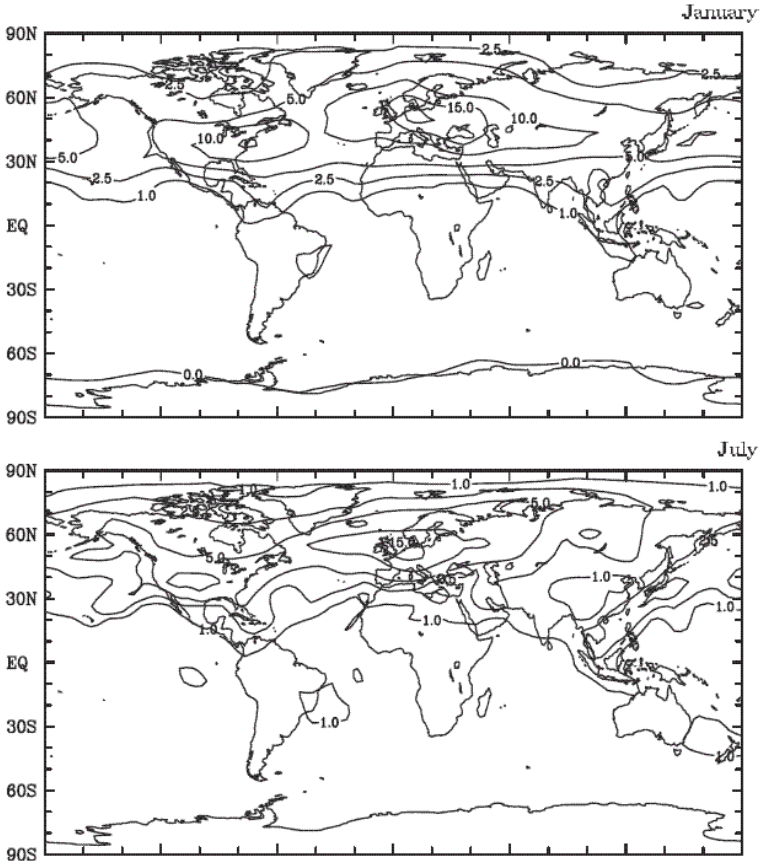

Fig. 21. Absolute decreases in aircraft-induced NO_x (in pptv) in January (top) and July (bottom) at 250 hPa due to plume modifications (Kraabøl et al., 2002).

GMDD
4, 137–196, 2011

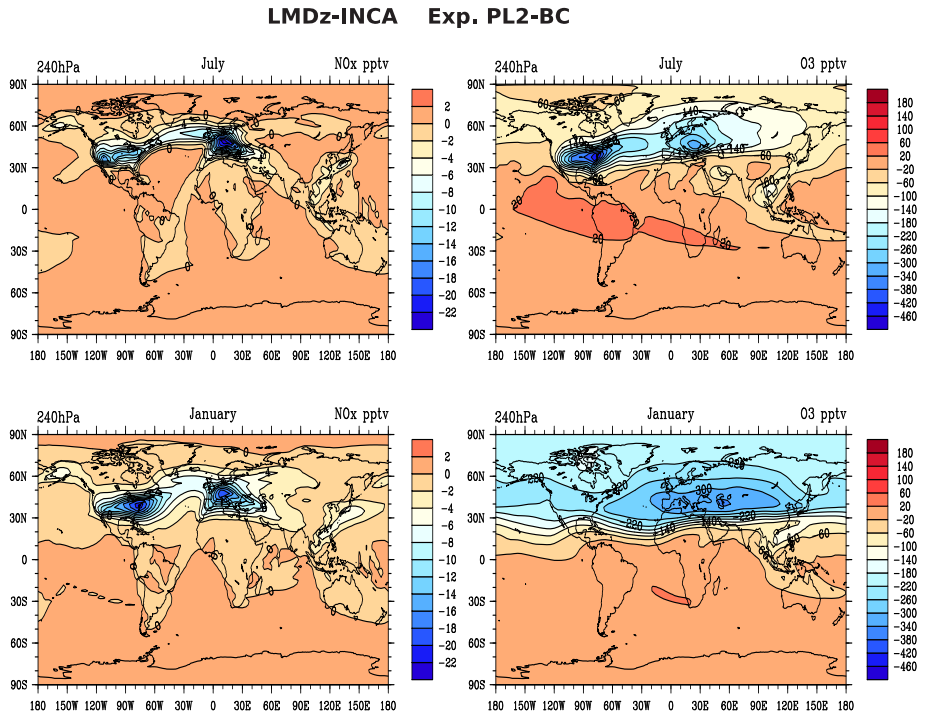

Fig. 22. LMDz-INCA model distributions of the NO_x (left) and O_3 (right) variations at 240 hPa in January (bottom panels) and July (upper panels) due to plume effects using the ERR method (Cariolle et al., 2009).

GMDD
4, 137–196, 2011

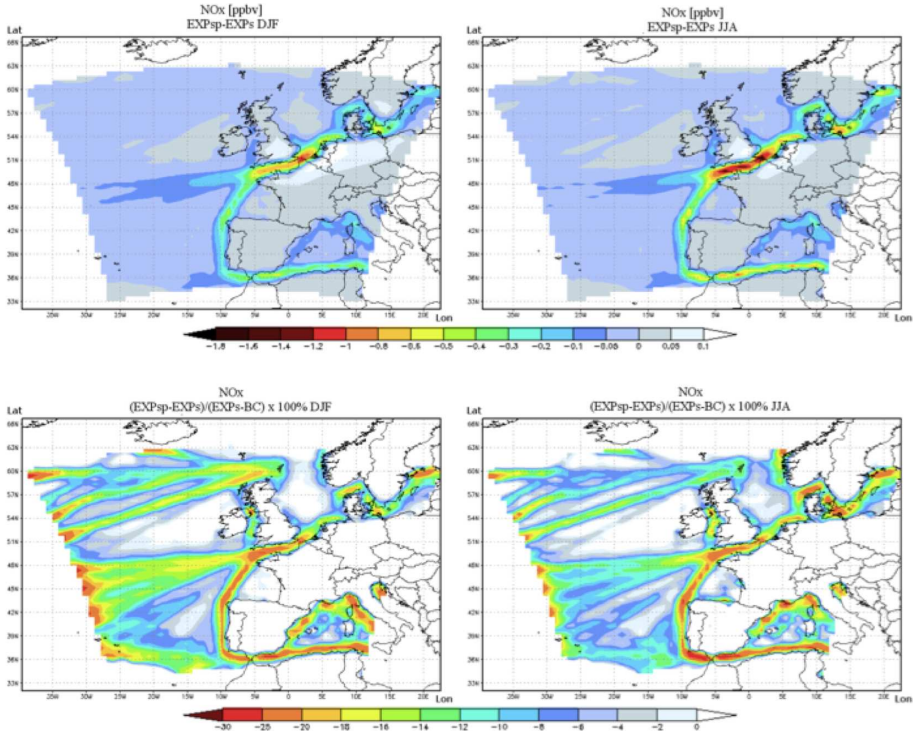

Fig. 23. Change in NO_x production by ship emissions (Huszar et al., 2010). Top panels: difference of surface NO_x of experiments with and without plume model, ε_{NO_x} (Eq. 55) in ppbv for winter (left) and summer conditions (right). Bottom panels: same but for relative change ε_{NO_x} (Eq. 56).

GMDD
4, 137–196, 2011